
Article:
Wang, R, Ji, Y, Colombera, L orcid.org/0000-0001-9116-1800 et al. (5 more authors) (2021) Axial and transverse depositional systems of a syn-rift basin fill (Bohai Bay Basin, China). Marine and Petroleum Geology, 128. 105045. ISSN 0264-8172

https://doi.org/10.1016/j.marpetgeo.2021.105045

Axial and transverse depositional systems of a syn-rift basin fill (Bohai Bay Basin, China)

Ru Wang[a,b], Youliang Ji[a], Luca Colombera[b], Nigel P. Mountney[b], Bo Yuan[c], Danjie Li[a], Hongyu Song[a], Sheng Zhou[a]

[a] *State Key Laboratory of Petroleum Resources and Prospecting, China University of Petroleum (Beijing), Beijing, 102249, China*

[b] *Fluvial, Eolian & Shallow-Marine Research Group, School of Earth & Environment, University of Leeds, Leeds, LS2 9JT, UK*

[c] *Research Institute of Exploration and Development, Zhongyuan Oilfield, Sinopec, China*

ABSTRACT

For improved prediction of reservoir distribution and quality in the infill of rift basins, it is paramount to characterize the extent and relative dominance of simultaneously active depositional systems fed by axial and transverse drainages, and to understand how these vary in response to geological controls. This study demonstrates how integration of seismic, wireline-log, core, petrographic and heavy-mineral datasets, combined with existing palaeotopographic reconstructions, can be utilized to characterize the spatiotemporal distribution and reservoir potential of syn-rift depositional systems associated with axial and transverse sediment routes to a lacustrine basin. In the Eocene of the Dongpu Depocentre (Bohai Bay Basin, China), three distinct delta types are identified: footwall-derived coarse-grained fan deltas and sand-rich deltas, and axial deltas that are dominated by siltstone and fine sandstone. The spatiotemporal distribution of these systems in the basin fill arose from the interaction of tectonic, lake-level, and climatic controls. Sedimentological and provenance analyses indicate the predominance (>85%) of axial systems over transverse systems in the infill of this elongate, asymmetrical graben. Locally, the interaction and amalgamation of transverse and axial systems was controlled by the presence of intra-basinal highs, through their influence on sediment-delivery pathways, and by high rates of sediment supply that caused overfill of isolated depocentres. Texturally mature, well-sorted fine sandstones of axial deltaic systems, which were sourced from comparatively large catchments, are attractive reservoir targets. By contrast, conglomerates of transverse fan deltas are poorly sorted and have more limited reservoir potential. However, footwall-derived fans may serve as viable reservoir targets locally, where fed by major hinterland drainages associated with long sediment-transport distances. Identification of the position of relay ramps in seismic data and recognition of bedrock-incised drainage outlets on the footwall basement of the basin margin may allow prediction of the presence and location of reservoir units associated with oversized deltas.

Keywords: provenance, delta, drainage basin, rift basin, source-to-sink, graben.

1. Introduction

The stratigraphic architecture of syn-rift basin fills can archive the interaction of axial and transverse sediment-delivery systems, fault-related topography, basin physiography, base-level variations and climate changes. Numerous subsurface and outcrop studies have focused on footwall-derived depositional systems, many examples of which are associated with multiple spatially distinct but coevally active entry points that deliver sediment to a basin, and for which several conceptual depositional models have been developed (e.g., Surlyk, 1978, 1984; Turner and Allen, 1991; Ravnås and Steel, 1997; Garland et al., 1999; Gawthorpe and Leeder, 2000; Jones et al., 2018; Turner et al., 2018). However, rift basins in which axial and transverse sediment-routing systems were active simultaneously and interacted in response to the interplay of allogenic and autogenic controls, are

comparatively poorly documented. Known examples include the East African Rift System (Soreghan et al., 1999; Zhang and Scholz, 2015), the Rio Grande Rift System (Leeder et al., 1996; Leeder and Mack, 2001), the Late Jurassic North Sea rift system (McLeod et al., 2002), the Corinth Rift, Greece (Gawthorpe et al., 2018; Cullen et al., 2019), and the Dampier Sub-basin, Australia (Chen et al., 2020). Understanding the relative dominance and interplay of axial and transverse depositional systems in syn-rift basins is of considerable significance for predicting hydrocarbon reservoir distribution and quality, particularly given that provenance dictates the composition of the accumulated sediment (Pettijohn et al., 1987; Johnson, 1993). Transverse syn-rift depositional systems are typically footwall-derived alluvial fans or fan deltas developed at the base of steep faulted scarps, sourced from catchments of limited size (e.g., Gawthorpe et al., 2018; Surlyk, 1978, 1984; Leppard and Gawthorpe, 2006; Chen et al., 2020). Although occasionally acting as productive reservoir units (Gawthorpe and Leeder, 2000), the deposits of these fan systems tend to be of restricted spatial extent, and typically comprise coarse-grained but poorly sorted deposits, which may have relatively poor reservoir potential (Schwarz and Wood, 2016; Gawthorpe et al., 2018; Somerville et al., 2020). Axial syn-rift fluvio-deltaic depositional systems are typically sourced from relatively larger catchments with longer transport distances. Thus, they tend to cover wider areas and to be characterized by relatively cleaner, finer-grained, better sorted, and more mature sediments, with relatively greater reservoir potential than their transverse counterparts (Schwarz and Wood, 2016; Sihombing et al., 2019). To assess and prioritize exploration targets in clastic hydrocarbon reservoirs, it is therefore important to consider the provenance and stratigraphic and spatial distribution of syn-rift depositional systems.

The aim of this study is to determine the distribution and reservoir potential of transverse and axial depositional systems and to investigate their controls. To accomplish this aim, an integrated subsurface study has been undertaken of the Eocene syn-rift interval of the Dongpu Depocentre (DDP) of the Bohai Bay Basin, China (Fig. 1), a mature hydrocarbon province for which substantial datasets of various type exist. A suite of seismic, wireline-log, core, petrographic and heavy-mineral datasets – combined with existing palaeotopographic reconstructions – have been utilized. Specific objectives of this work are as follows: (i) to characterize the sedimentological characteristics and stratigraphic architecture of syn-rift depositional systems of a lacustrine basin; (ii) to illustrate the application of an integrated sedimentological and provenance study to the reconstruction of the relative dominance and interaction of axial and transverse sediment-routing systems in syn-rift basin fills; (iii) to develop a better understanding of geological controls on syn-rift sedimentation and on the relative preservation of associated axial and transverse depositional systems.

2. Geological setting

The Bohai Bay Basin (BBB) is a Cenozoic continental rift basin developed in the North China craton (Li et al., 2012; Zhu et al., 2020; Fig. 1A). This basin is surrounded by the Taihang Range to the west, the Yanshan Range to the north, the Ludong Uplift to the east and the Luxi Uplift to the south (Fig. 1B). The pre-Cenozoic basement of the BBB has been dissected by a series of normal faults and minor strike-slip faults trending NE-NNE, NW-WNW, and E-W respectively (Fig. 1B). The basement mainly comprises of sedimentary rocks (Jurassic–Cretaceous, Carboniferous–Permian, Cambrian–Ordovician, and Middle to Upper Proterozoic) and crystalline metamorphic rocks (Lower Proterozoic and Archean crystalline-metamorphic rock) (Qi and Yang, 2010). The Dongpu Depocentre (DPD) is part of the BBB; its development has been controlled by a series of NNE-SSW-trending normal faults (Zhang et al., 2007). The DPD is located in the Southern Bohai Bay Basin, China (Fig. 1A), and is surrounded by the Luxi Uplift to the east, the Neihuang Uplift to the west, the Lankao Uplift to the south and the Shenxian Sag to the north (Fig. 1C). The depocentre takes the form of an asymmetric graben, bounded to the east by the NW-dipping Lanliao Fault system and to the west by the SE-dipping Changyuan-Shijiaji-Songmiao Fault system (Fig. 1C; Fig. 2B). The DPD can be divided into five elongated structural units limited by the main basin-bounding fault systems and by the intrabasinal NNE-SSW-striking Huanghe-Wenxi-Guancheng Fault: the Western Slope zone, the Western Trough, the Central Uplift, the Eastern Trough and the Lanliao Fault zone (Chen et al., 2007; Jiang et al., 2008; Fig. 1C).

As revealed by 2D seismic lines and borehole data, the DPD contains a Cenozoic succession that is over 7 km thick (Yu et al., 2012; Fig. 2). Cenozoic rifting, which commenced in the early Eocene and continued until the end of the Oligocene (Zhang et al., 2007; Zhu et al., 2020), comprised four stages:

(i) early syn-rift stage (Member 4 of Shahejie Formation; Es_4), (ii) main syn-rift stage (Member 3 of Shahejie Formation; Es_3), (iii) transition to late syn-rift stage (Member 2 and Member 1 of Shahejie Formation; Es_2 and Es_1) and (iv) late syn-rift stage (Dongying Formation; Ed) (Hou et al., 2001; Su et al., 2006; Fig. 2). During the early syn-rift stage, the Lanliao Fault system at the eastern edge of the basin was activated. This stage was associated with deposition of alluvial-fan and lacustrine deposits characterized by interbedded purple, reddish mudstone and sandstone on the hangingwall of the Lanliao Fault (Ji et al., 2005b; Yu et al., 2012). The main syn-rift stage was characterized by strong tectonic activity of most faults in the depocentre, and by the formation of the Central Uplift. This stage was associated with the accumulation of fan-delta, deltaic, lacustrine and gravity-flow-dominated deposits. Deposits of these systems are characterized by interbedded dark-grey mudstone, pale-grey siltstone and sandstone in the intrabasinal area, and by conglomerates in marginal areas (Yu et al., 2012). During the transition to the late syn-rift stage, the upheaval of the Central Uplift ceased, resulting in the deposition of fluviolacustrine interbedded reddish or grey mudstone and siltstone (Yu et al., 2012). During the late syn-rift stage, the depocentre was dominated by fluvial systems recorded in the Dongying Formation (Yu et al., 2012). Following deposition of the Dongying Formation, tectonic activity waned dramatically; from the late Cenozoic to the present day, continued basin evolution has been via regional thermal subsidence.

The focus of this study is the Member 3 of the Shahejie Formation (Es_3 hereafter), which was accumulated during the main syn-rift stage. In the study area, based on the integration of core, well-log and seismic data (cf. Vail et al., 1977), this succession has been divided into three third-order sequences (SQ3, SQ4 and SQ5), six systems tracts (Fig. 2A), and 27 higher-scale units classified as parasequences, according to Ji et al. (2016). The specific sandstone units of interest in this study are termed by petroleum geologists working on the stratigraphy of the basin fill as (from bottom to top): *Lower Es_3 1st sandstone unit, Middle Es_3 9th sandstone unit, Middle Es_3 8th sandstone unit*, *Middle Es_3 6th sandstone unit*, *Middle Es_3 5th sandstone unit* and *Upper Es_3 8th sandstone unit*. These units, each of which corresponds to a parasequence according to Ji et al. (2016), are termed units F to A in this work for simplicity (Table 1).

Table 1. Correspondence between the nomenclature of sandstone units of the Member 3 of the Shahejie Formation used by the local oil industry and abbreviations used in this work. Es_3 = Member 3 of Shahejie Formation.

Local sandstone-unit nomenclature	Abbreviation used in this work
Upper Es_3 8th sandstone unit	Unit A
Middle Es_3 5th sandstone unit	Unit B
Middle Es_3 6th sandstone unit	Unit C
Middle Es_3 8th sandstone unit	Unit D
Middle Es_3 9th sandstone unit	Unit E
Lower Es_3 1st sandstone unit	Unit F

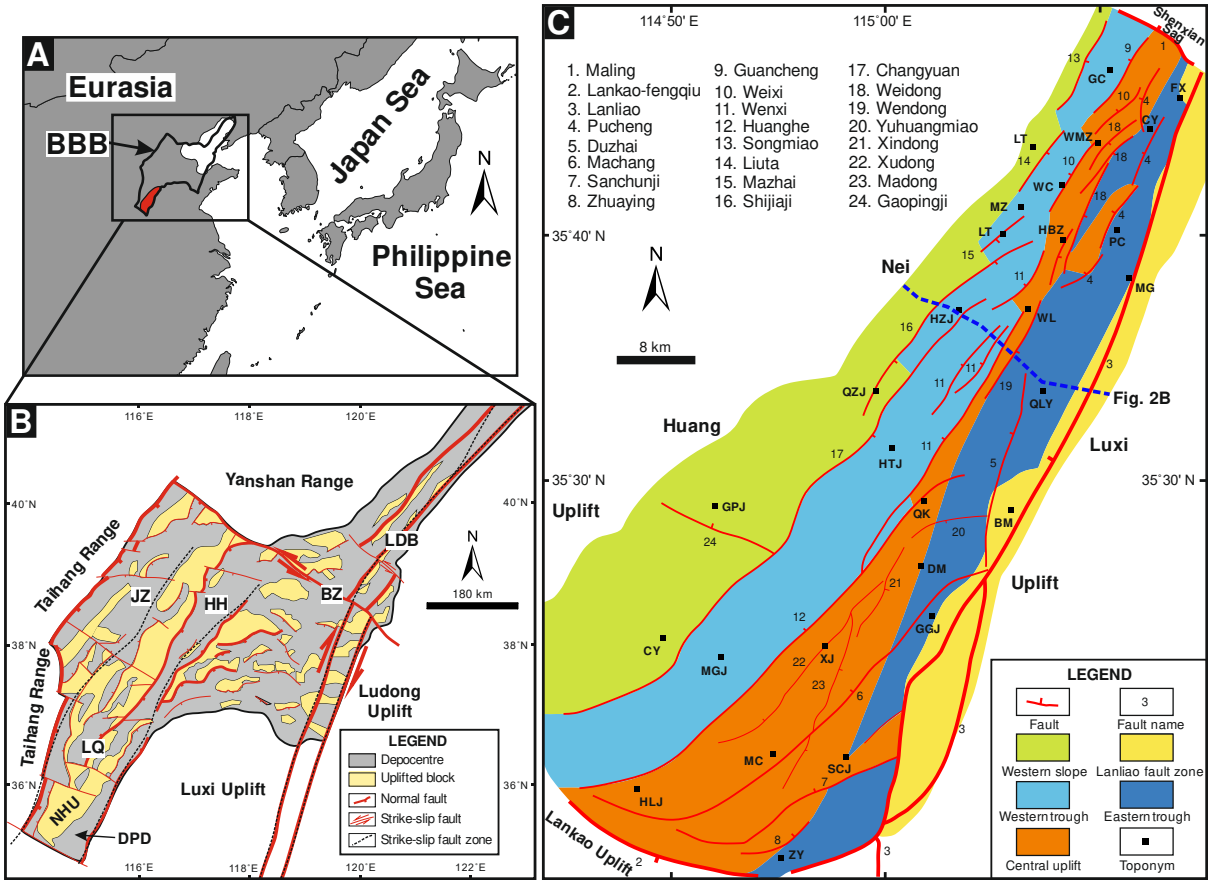

Fig. 1. (A) Location of the Bohai Bay Basin and Dongpu Depocentre (China). The red polygon indicates the study area (Dongpu Depocentre). (B) Schematic structural map of the Cenozoic Bohai Bay Basin. Modified from Qi and Yang (2010) and Zhu et al. (2020). (C) Regional map illustrating the main structural elements and faults of the Dongpu Depocentre. Modified from Chen et al. (2007). The position of the interpreted seismic section across the study area shown in Fig. 2B is indicated (blue dashed line). Note that the western basin boundary of the DPD is mainly controlled by the SE-dipping Changyuan-Shijiaji-Songmiao Fault system. The transition between the western part of the basin and Neihuang Uplift to the west is gradual after passing the Changyuan-Shijiaji-Songmiao Fault system. The exact location of the western boundary of the basin is thus determined by the sediment pinch-out of the sediment fill in the basin recognized in seismic profiles. BBB = Bohai Bay Basin; BM = Baimiao; BZ = Bozhong Sub-basin; CY = Changyuan; CY = Chenying; DM = Dongming; DPD = Dongpu Depocentre; FX = Fanxian; GC = Guancheng; GGJ = Gegangji; GPJ = Gaopingji; HBZ = Hubuzhai; HH = Huanghua Sub-basin; HLJ = Huanglingji; HTJ = Haitongji; HZJ = Huzhuangji; JY = Jiyang Sub-basin; JZ = Jizhong Sub-basin; LDB = Liaodong Bay Sub-basin; LQ = Linqing Sub-basin; LT = Liuta; LT = Liutun; MC = Machang; MG = Maogang; MGJ = Menggangji; MZ = Mazhai; NHU = Neihuang Uplift; PC = Pucheng; QK = Qiaokou; QLY = Qianliyuan; QZJ = Qingzuji; SCJ = Sanchunji; WC = Weicheng; WL = Wenliu; WMZ = Wenmingzhai;
XJ = Xuji; ZY = Zhuaying.

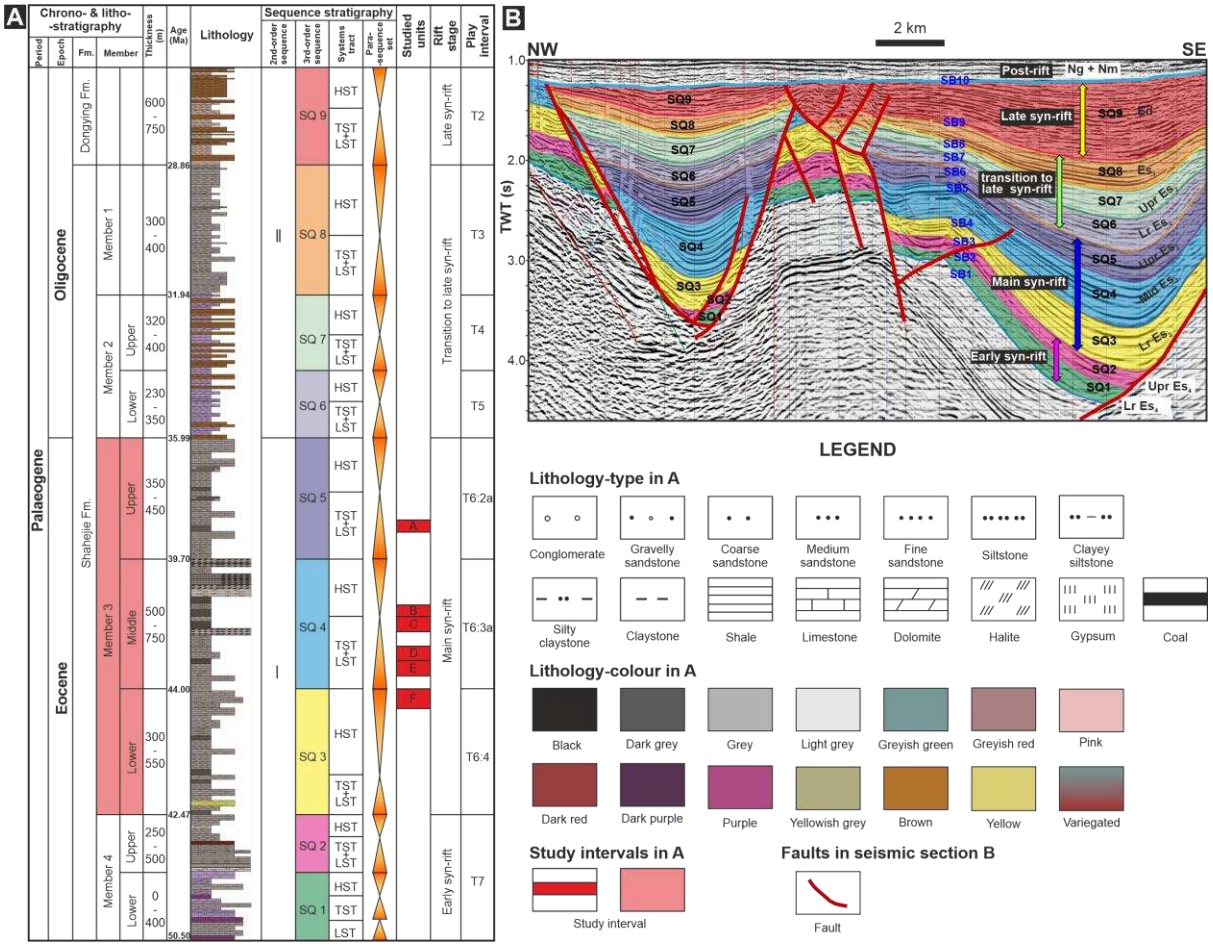

Fig. 2. Schematic stratigraphic column for the Dongpu Depocentre (A) and interpreted seismic-stratigraphic section presented on a NW-SE direction (B). Modified from Ji et al. (2016) and Yu et al. (2012). Location of this seismic section is indicated in Fig. 1C. Note that the interval of interest in this study is Member 3 of Shahejie Formation (Es_3), which developed in the main syn-rift stage. Red bands denote the units studied in this work, and termed F to A in this article (see Table 1 for correspondence to local nomenclature). SB = Sequence Boundary; SQ = Sequence; LST = Lowstand Systems Tract; TST = Transgressive Systems Tract; HST = Highstand Systems Tract; Es = Shahejie Formation; Ed = Dongying Formation; Ng = Guantao Formation; Nm = Minghuazhen Formation; Lr = Lower; Mid = Middle; Upr = Upper; TWT = two-way travel time. Tectonic events from Zhang et al. (2007) and Zhu et al. (2020).

3. Dataset and methodology

In this study, a combination of seismic, wireline-log, core, petrographic and heavy-mineral data was used. This work utilizes full-stack 3D seismic reflection data, which cover an area of ca. 5,300 km^2 (Fig. 3). Within the stratigraphic interval of interest, the seismic data have a dominant frequency of ca. 20 Hz, and the average interval velocity is of ca. 3,040 m/s, resulting in a vertical seismic resolution in the study interval of ca. 38 m, and in horizontal resolution of 30-61 m. Seismic interpretation was performed using Geoframe 2016. Cuttings from ca. 1,400 wells and wireline logs from 526 wells that penetrate the Es_3 interval were examined (Fig. 3), and well ties were utilized to refine seismic interpretations. Wireline-log interpretation was carried out using Resform 2016 based on the log-responses from a series of logging tools (spontaneous potential [SP], gamma ray [GR], resistivity, conductivity, acoustic impedance, bulk density, and neutron porosity). Sedimentary logging of ca. 2,000 m of core from 50 wells (Fig. 3) penetrating the studied interval was performed at 1:40 scale.

Cored sections were utilized to describe sedimentary facies and facies associations. Classification schemes for facies and facies associations, reflecting representative physical sedimentary processes and

depositional environments, were constructed for the study area based on core and wireline-log characteristics. These observations were then integrated with seismic interpretations and related to wireline-log characteristics. In regions covered by relatively few widely dispersed boreholes (Fig. 3), seismic data were analysed through planform seismic-attribute mapping to enable the identification of features that are significant in terms of seismic geomorphology. The main attributes considered in this work are spectral decomposition, Root Mean Square (RMS) amplitude, average energy, magnitude of curvature and acoustic impedance from seismic inversion. The interpretation of attribute maps was calibrated by comparison with the analysis of cross-sectional seismic facies and using well-to-well correlation panels.

Isopach maps showing spatial variations in the thickness of sandstone or siltstone were created for each study intervals (units A-F) based on data from well cuttings or wireline logs of 947 wells. The spatial distributions of values of sandstone or siltstone fraction (i.e., the ratio between the cumulative thickness of sandstone or siltstone and the thickness of the overall interval) were mapped for each study interval (Lower Es_3, Middle Es_3 and Upper Es_3) based on data from 810 wells. The mapping of the distribution of sandstone and siltstone in the basin allows estimation of the sediment budget associated with different sediment-delivery routes.

One-hundred-and-sixty-five thin sections of sandstone or siltstone samples of the cored wells were used to undertake petrographic analyses, which were supplemented with petrographic data obtained from unpublished well reports. All sample processing and slide analysis was carried out at China University of Petroleum (Beijing). Heavy mineral data from 161 wells gathered from well reports are utilized to investigate sediment provenance of the DPD for each study interval (Lower Es_3, Middle Es_3 and Upper Es_3), integrated with petrographic data, sandstone or siltstone fraction distributions, analysis of potential source areas and existing palaeotopographic reconstructions of the DPD (Lower Es_3, Middle Es_3 and Upper Es_3) obtained from the Exploration and Development Research Institute of Zhongyuan Oilfield, Sinopec, China. These palaeotopographic maps were constructed following the approach by Lin et al. (2009). This is based on (i) seismic flattening of regionally extensive condensed mudstone layers that mark maximum flooding surfaces, (ii) derivation of the original depositional thickness of target intervals from the present-day thickness observed in the 3D seismic data, corrected for erosion, utilizing the seismic reflection configuration and well-log comparison approach (Wyllie et al., 1956; Kumar, 1979; Henry, 1996), and through decompaction (Athy, 1930), and (iii) calibration with palaeo-bathymetry inferred from palaeontological data.

All contour maps in this study were created through inverse-distance interpolation of punctual values, using Surfer® (Golden Software, LLC). These maps were originally constructed for areas extending beyond the region of the input data coverage by using the inverse-distance interpolation algorithms of the software. The contour maps were subsequently checked and revised to remove unrealistic values. For example, seismic-attribute data were used to assist the mapping of sandstone or siltstone thickness distributions for regions covered by few boreholes.

Previous studies on the palaeogeography of the DPD either focused on a single fault block or basin-scale mapping of the DPD for member-scale stratigraphic units (e.g., Ji et al., 2005b, 2016; Yu et al., 2012). In this work, palaeogeographic maps are reconstructed for each study interval (units A-F), in part using information from previous studies of the DPD, but also incorporating original datasets described above; each map represents the gross depositional environments for each study interval.

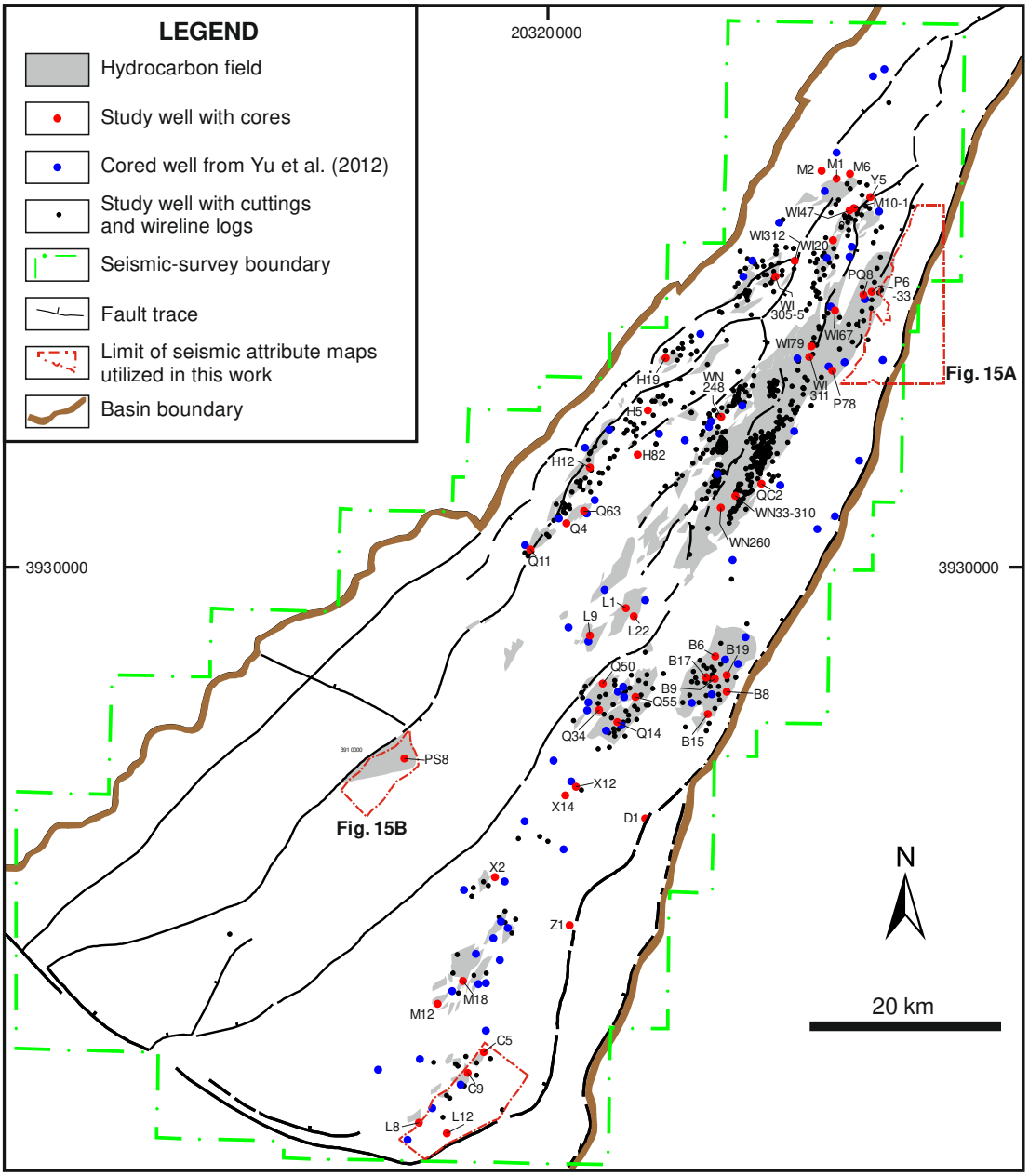

Fig. 3. Map illustrating location of studied boreholes (cuttings and wireline logs) and cores, the coverage of the seismic dataset (green dashed line) and the location of the seismic attribute maps (red dashed lines) utilized in the present study. The location of hydrocarbon fields in the studied area is also shown.

4. Results

4.1 Sedimentological analysis of depositional systems of the DPD

Eighteen sedimentary facies are identified in cored intervals; detailed descriptions are provided in Table 2 and representative core photos are shown in Figure 4. The facies are arranged into fourteen facies associations (FAs), which are themselves representative of four main depositional environments: footwall-derived coarse-grained fan deltas, axial fine-grained deltas, footwall-derived sand-rich deltas and open lake. These four depositional environments are interpreted based on core, wireline-log and seismic data, and with consideration of existing information available from previous palaeographic studies of the DPD (Ji et al., 2005b, 2016; Yu et al., 2012); the classification of the depositional environments is also partly based on their location relative to structural features of the basin. A summary

of the depositional environments and of their component facies associations is provided below. Detailed descriptions and interpretations are presented in Supporting Information 1 and Table 3.

Table 2. Facies descriptions and interpretations. The facies codes are adapted and extended from those by Miall (1996). Information on the composition of clasts in conglomerates is not detailed here, since it varies significantly across the extent of the basin (see Table 4). LFR = lower flow regime; UFR = upper flow regime; ⌀ = diameter.

Facies code	Facies type	Facies description	Process interpretation
Gc1	Clast-supported conglomerate (type 1)	Moderately sorted, clast-supported, granule-pebble grade conglomerates. Clasts are mainly extraformational, well-rounded to sub-rounded and of varying sizes (typically ⌀ = 1-3 cm, ⌀ max = 8 cm). Clast b-axis imbrications [a(t), b(i); cf. Davies and Walker, 1974] and faint cross stratification are common. Matrix is dominated by coarse-grained to fine-grained sandstone (feldspathic litharenite). Commonly erosional bases with lags of sub-rounded cobbles (> 5 cm). M-thick beds.	Sediment textures, ordered imbrications [a(t), b(i)] and the presence of faint cross-stratifications are indicative of bedload traction (Davies and Walker, 1974; Allen, 1982).
Gc2	Clast-supported conglomerate (type 2)	Poorly sorted, clast-supported, granule-cobble grade variegated or greenish-grey conglomerates with floating cobbles in the lower part of beds. Sub-rounded to sub-angular clasts (< 10 cm). Commonly normally graded to fine-grained sandstones. Rare ordered imbricated fabrics [clast a-axis imbrications; a(p), a(i); cf. Davies and Walker, 1974] in the lower part of the beds. Dm- to m- thick beds.	Rapid deposition by non-cohesive debris flows and/or high-concentration gravel- and sand-laden flows. The lower conglomeratic portion with local [a(p), a(i)] fabric is characteristic of highly concentrated grain dispersions subject to intense laminar shear stress (Rees, 1968, 1983; Allen, 1982), and may reflect deposition by viscous debris flows (*sensu* Lowe, 1982; Surlyk, 1984). Normal grading reflects suspension settling of gravel- and sand-laden flows during waning conditions (Allen, 1982). These vertical changes may reflect transformation of debris flows through dilution (cf. Fisher, 1983; Potsma et al., 1988).
Gm	Matrix-supported conglomerate	Poorly sorted, matrix-supported, granule-cobble grade variegated or greenish-grey conglomerates. Sub-angular clasts with vary sizes (< 10 cm). Disordered fabric. Occasionally inverse grading in the lower part of the beds. Dm- to m- thick beds.	Rapid deposition from debris flows or hyperconcentrated flows (Fisher, 1971; Lowe, 1982; Surlyk, 1984). The lower inversely graded part is possibly formed by freezing of a traction carpet or viscous debris flow with high shear tress in the basal zone (cf. Middleton, 1970; Postma et al., 1988).
Sm	Massive and crudely laminated sandstone (type 1)	Fine, medium, coarse to very-coarse sandstones with no apparent internal structures. Locally gravel lags and/or pebble clusters are present at the base of the bed.	Product of the rapid deposition of sediment whereby no bedform develops during the sedimentation process (Arnott and Hand, 1989; Kneller and Branney, 1995).

Sg	Normally or inversely graded sandstone	Very-fine to very-coarse sandstones with inverse or normal grading. Mainly massive structure, but rarely with some faint laminations. Cm- to dm-thick beds.	Product of the rapid deposition by sand-laden turbulent flows during waning or waxing flow conditions (Bouma, 1962; Kneller, 1995). In some cases, inverse grading might be associated with waxing hyperpycnal flows (Mulder et al., 2001; Mulder et al., 2003).
St	Trough cross-stratified sandstone	Fine to medium sandstones with well sorted and well-rounded grains. Set thickness with cm- to dm-thick scale. Locally gravel lags and/or pebble clusters are present close to the bases of beds.	Down-current migration of sinuous-crested (3D) dunes driven by unidirectional flow (LFR) (Allen, 1982, 1985).
Sp	Planar cross-stratified sandstone	Well sorted, well rounded fine to medium sandstones. Set thickness with cm- to dm-thick scale. Locally gravel lags and/or pebble clusters are present close to the bases of beds.	Down-current migration of straight-crested (2D) dunes driven by unidirectional flow (LFR) (Allen, 1982, 1985).
Sh	Parallel-laminated sandstone	Greyish fine to medium sandstones with well sorted, moderately rounded grains and parallel laminations. Rare primary current lineation on the bedding surfaces. In some cases, silty laminae can be observed. Locally gravel lags and/or pebble clusters are present close to the bases of beds.	Product of deposition in either the upper or lower flow regime plane-bed field (Bridge and Best, 1988; Best and Bridge, 1992).
Sl	Low-angle cross-bedded sandstone	Greyish fine to medium sandstones with well sorted, moderately rounded grains and low-angle (< 15°) cross-bedding. Locally gravel lags and/or pebble clusters are present close to the bases of beds.	Formed due to deposition either in the upper or lower flow regime plane-bed fields on pre-existing low-relief topography, or by traction (with or without fall-out to deposit the silty laminae) driving migration of low-relief bedforms. In the latter case, these deposits might develop under conditions transitional between the lower and upper-flow regimes in association with bedforms such as washed-over dunes (cf. Fielding, 2006).
Src	Current ripple-laminated sandstone	Very-fine to silty sandstones with ripple laminations (0.5-1 cm laminae).	Migration of ripple forms driven by unidirectional current (LFR) (Allen, 1963, 1968).
Srw	Wave ripple cross-laminated sandstone	Very-fine to silty sandstones with well sorted, well-rounded grains and wave-ripple cross laminations. Commonly symmetric ripple marks with peaked and straight crests, rounded troughs can be observed on upper bedding surfaces.	Migration of ripple forms in wave-driven oscillatory flows at low to moderate flow velocities (LFR), at a water depth between the mean fairweather wave base and the mean lake level (Allen, 1979, 1981).
Shcs	Hummocky cross-stratified sandstone	Light-grey fine sandstones with hummocky cross-stratification. Dome-shaped surfaces are commonly preserved, with wave-reworked tops.	Formed under a combination of unidirectional and oscillatory flow associated with storm conditions. Deposition includes fall-out from suspension and lateral tractional flow due to wave oscillation. Typically develops in shallow-water environments at a water depth between the mean fairweather wave base and the

			storm wave base (Dott and Bourgeois, 1982; Leckie and Walker, 1982; Walker et al. 1983; Myrow and Southard, 1996; Jelby et al. 2020).
Sd	Soft-sediment deformed sandstone	Very fine sandstones or silty sandstones with load casts, ball-and-pillow structures, convolute laminations, dish-and-pillar structures, overturned cross-bedding, and other forms of soft-sediment deformation.	Formed due to post-depositional deformation of sediments prior to lithification, possibly relating to liquefaction and fluidisation (cf. Owen, 1995).
Fr	Reddish laminated to massive mudstone	Parallel-laminated or massive mudstones. Dark-red or purple colour. Cm- to m-thick beds. Rare desiccation cracks.	Suspension fall-out in oxic bottom conditions. The red colour might reflect the state of the oxidation of the parent material, which was oxidised subaerially (under conditions of low water table) before being transported to the lake.
Fc	Organic-rich dark-grey and black laminated to massive mudstone	Parallel-laminated or massive mudstones. Black or dark-grey coloured. Organic rich. Abundant in plant debris. Cm- to m-thick beds.	Suspension fall-out in anoxic bottom conditions.
Fl	Interlaminated very fine sandstone, siltstone and claystone	Interlaminated very-fine sandstone, siltstone and claystone. Rare thin cross-laminated sandstone lenses.	Suspension deposits from hypopycnal or homopycnal flows, and intermittent deposition by flood-generated hyperpycnal flows (Mulder et al., 2003).
Hg	Halite, gypsum, gypsiferous salt, gypsiferous mudstone	Salt beds, gypsum beds, gypsiferous salt and gypsiferous mudstone. Gypsum occurs in flakey or banded shapes.	Either formed by lake desiccation due to evaporation within an arid climatic setting (Nadon and Middleton, 1985; Allen, 1985) or formed by evaporite precipitation in a deep perennial saline-lake environment (Sirota et al., 2018)

Fig. 4. Core photographs illustrating the facies types described in this study. (A) Clast-supported conglomerate with imbricated clasts and faint cross-stratification (Gc1), well D1, 4306.72 m. (B) Matrix-supported conglomerate with disordered fabric (Gm), well WI311, 3602.63 m. (C) Massive coarse-grained sandstone (Sm), well D1, 4306.27 m. (D) Massive, clean, fine-grained sandstone with crude laminations (Sm), well WI311, 3613.48 m. (E) Trough cross-stratified very fine-grained sandstone with silty laminae (St), well WI47, 2906.20 m. (F) Trough cross-stratified clean fine-grained sandstone (St), well WN33-310, 3721.5 m. (G) Parallel-laminated fine-grained sandstone (Sh), well WI20, 2428.60 m. (H) Ripple-laminated sandstone (Src) with climbing ripple laminations on the top, flaser bedding and wavy bedding on the bottom, well WN19-5, 2799.40 m. (I) Ripple-laminated sandstone with symmetric ripples having peaked crests and rounded troughs (Srw), well WN260, 3562.20 m. (J) Hummocky cross-stratified sandstone (Shcs), well WN95, 2633.90 m. (K) Ripple-laminated sandstone with wavy bedding and lenticular bedding (Sr), well Q44, 3252.61 m. (L) Soft-sediment deformed sandstone with small detached load balls and pillows sinking into underlying mudstone (Sd), well Q15, 3377.03 m. (M) Soft-sediment deformed sandstone with dewatering structure (Sd), well WN33-310,3767.08 m. (N) Soft-sediment deformed sandstone with load cast and adjacent flame structure (Sd), well WN33-310, 3720.09 m. (O) Injected sandstone into overlying mudstone, well

X14, 4331.95 m. (P) Injected sandstone into overlying mudstone, well X14, 4331.10 m. (Q) Interlaminated very fine sandstone, siltstone and claystone (Fl) with load casts and flame structures at the base, well H12, 2305.80 m. (R) Reddish massive mudstone, well PS8, 3239.92 m. (S) Organic-rich dark-grey laminated mudstone (Fc) with abundant plant debris and pyrite, well WI79, 3401.09 m. (T) Light-yellow cubic halite crystals within grey silty claystone (Hg), well WN13-367, 3043.50 m. (U) Massive colourless halite layers (Hg), well WN248, 3393.15 m. (V) Interlaminated grey mudstone and gypsum layers (Hg), well WN248, 3380.90 m. The scale bar is 5 cm in all cases.

Table 3. Depositional environment and component facies association descriptions present in this study.

Depositional environment	Facies association	Thickness	Constituent facies	FA description	Relationships with other deposits	Wireline-log signature	FA interpretation	Seismic expression
Footwall-derived coarse-grained fan delta (topsets only identified in core)	Channel fill	Typically 10 m, ranging from 2 to 15 m.	Gc1, Gc2, Sg, Sm	This FA constitutes the largest proportion of the coarse-grained delta-topset deposits (ca. 70-90%). Two variants of this FA could be identified in core, indicated as A and B below. (A) Predominantly moderately sorted, clast-supported, granule-pebble grade conglomerates (facies Gc1 in Table 2; Fig. 5D). The clasts are mainly extraformational, well-rounded to sub-rounded and of varying sizes (typically ⌀ = 1-3 cm, ⌀ max = 8 cm). Conglomerates in this type of channel fills typically display ordered imbricated fabric [a(t), b(i)] and faint cross-stratifications. The matrix is dominated by coarse-grained to fine-grained sandstones. This succession commonly fines upwards into fine-grained sandstones or siltstones with erosional bases overlain by lags of sub-rounded cobbles (⌀ > 5 cm). In places, wood fragments and plant debris can be observed. The sandstones are dominantly of moderately sorted, sub-rounded to sub-angular grains in texture (Fig. 5D), are feldspathic litharenites in composition, display linear grain contacts, and are mainly cemented by dolomite and authigenic clay mineral. (B) Poorly sorted, clast-supported, sandy granule-cobble grade variegated or greenish-grey conglomerates with rare crude laminations and [a(p), a(i)] fabric; facies Gc2 in Table 2; Fig. 5. In places, floating cobbles are present near the base of beds (Fig. 5C). The clasts are predominantly sub-rounded to sub-angular, rarely well rounded and of varying sizes (⌀ < 10 cm). The matrix is typically composed of sub-angular to angular, fine to coarse sandstones. This succession typically normally grades to fine-grained sandstones upward. The bed bases are highly erosional or sharp.	In sharp erosional contact with underlying fine-grained delta-plain deposits and sharply or gradationally overlain by fine-grained delta-plain deposits. The relationships with potential underlying foreset deposits could not be observed in the available cores.	Bell-shaped, barrel-shaped or serrated bell-shaped, barrel-shaped log motifs starting at channel base. GR values increase upward from the channel-fill base (50-140 API).	This FA is interpreted as alluvial channel fills. The clast size, moderate sorting, clast-supported nature and ordered imbrications [a(t), b(i)] and presence of faint cross-stratifications, together with erosional basal contacts and association with fine-grained delta-plain deposits, make this FA of variant A interpretable as the product of bedload transport by high-energy gravel-rich streamflows (Davies and Walker, 1974; Allen, 1982). The limited compositional and textural maturity suggests limited transport distance. The FA of variant B is interpreted as alluvial channel fills that record deposition from non-cohesive debris flows or hyperconcentrated flows. Clast-supported, massive conglomerate with rare clast a-axis imbrications [a(p), a(i)] are interpreted to be deposited from highly concentrated, viscous debris flows (*sensu* Lowe, 1982; Surlyk, 1984). Beds with normal grading are produced by suspension settling of gravel- and sand-laden flows during waning conditions (Allen, 1982). Vertical changes in the deposits may reflect debris-flow transformation through dilution (cf. Fisher, 1983; Potsma et al., 1988).	Medium amplitude, moderate continuity, steep-dipping reflections. Internal reflections are commonly chaotic. 3D prism-apron shape along the fault. Radially distributed features are seen in plan view, which possibly represent channel bodies. Typically positioned directly on top of the hangingwall of the main basin-bounding fault and dipping away from the fault.
	Delta plain	up to 10 m	Fr, Fc, Fl	Reddish or medium-grey laminated or massive mudstones and siltstones. Locally cm-thick, red palaeosols or plant debris can be seen.	Occurs in association with channel-fill conglomerates.	Serrated log motif with a high positive response (140 API).	The characteristics of this FA and its association with coarse-grained channel-fill deposits make this FA interpretable as delta-plain fluvial topset deposits. Laminated or massive mudstones and siltstones indicate deposition in a low-energy environment, due to suspension fall-out in oxic or anoxic bottom conditions. The reddish colour might reflect parent materials that were oxidised subaerially, possibly before being transported to submerged areas with oxic bottom conditions. The occurrence of cm-thick, red palaeosols indicates occasional subaerial exposure.	
Footwall-derived sand-rich delta	Distributary channel	up to 10 m	St, Sp, Srw, Src, Sm, Sc, Sg	Mainly fine, medium and coarse sandstones with predominant cross stratifications and subordinate parallel laminations. The bed bases are highly erosional with abundant intraformational clasts (mudstone rip-up clasts) and poorly sorted pebble clusters. The FA typically fines upward from massive sandy granule-pebble grade conglomerates, through massive/graded coarse-grained sandstones, to parallel-laminated medium sandstones, cross-bedded sandstones, culminating to fine-grained sandstones or siltstones with crude laminations or wave/ripple laminations (Sm, St, Sp, Srw and Src in Table 2; Fig. 6). Petrographic analysis indicates the sandstones are predominantly feldspathic litharenites and lithic fragments are dominated by limestone.	Erosional base typically incising fine-grained interdistributary bay/swamp deposits or mouth bar deposits. Overlain by interdistributary bay/swamp deposits.	Bell-shaped, barrel-shaped or serrated bell-shaped, barrel-shaped log motifs starting at channel base. Sometimes forms the upper part of a symmetrical log motif. GR values increase upward (8-14 API). Low GR values possibly due to the proximity with salt layers.	This FA is interpreted as the record of high-energy active distributary channels. Sandstones of feldspathic litharenites in composition and lithic fragments dominated by limestone imply provenance from a nearby landmass. Highly erosional surfaces overlain by poorly sorted, massive conglomerates may represent deposition by debris flows or hyperconcentrated flows during flood events.	Medium amplitude, discontinuous, dipping reflections that are separated by high amplitude, flat-lying reflections. Low-angle, basinward dip with clinoformal shape. Foresets display a highly progradational stacking pattern. Foresets are dominantly constrained to a single interval and are confined laterally. Predominantly positioned in the immediate hangingwall of the border fault and dipping away from the fault.
	Interdistributary bay/swamp	up to 10 m	Fl, Fc, Srw, Src	Predominantly interlaminated dark-grey mudstones and muddy siltstones with rare current and wave ripples.	Occurs in association with distributary channel sandstone facies association.	Serrated log motif. Higher GR values than distributary channel deposits (14 API). Low GR values possibly due to the proximity with salt layers.	This FA is interpreted to represent suspension fall-out in a low-energy interdistributary bay environment, with floods generating rare bedforms. Black and dark-grey organic rich parallel-laminated fine-grained facies reflect suspension fall-out in anoxic bottom. The presence of thin coal beds, plant debris and pyrite nodules support a reducing environment. Occasional thin siltstone beds with rare current and wave ripples may record deposition from tractive currents in crevasse channels and crevasse splays into backswamp areas. Together with the association with coarser-grained distributary channel fills, this indicates deposition in an interdistributary-bay and swamp environment.	
	Mouth bar	< 5 m	St, Sp, Sh, Sl, Src, Srw	Predominantly fine to medium sandstones with well sorted, well rounded grains and abundant cross stratifications. Commonly the FA displays a gradationally coarsening upward grain-size profile from thinly bedded parallel-laminated and current-ripple laminated siltstones to cross-stratified or massive fine to medium sandstones (St, Sp, Sh, Sl, Src and Srw in Table 2; Fig. 6A).	Typically underlain gradationally by pro-delta parallel-laminated dark-grey mudstones and siltstones or delta-front alternations of very fine sandstones and mudstones. Overlain by coarser-grained cross-bedded or massive sandstones of distributary-channel or crevasse-channel origin or by finer-grained delta-plain deposits.	Funnel-shaped or serrated funnel-shaped log motif. Sometimes forms an integral part of the symmetrical log motif.	Sandstones of high compositional and textural maturity with dominant traction-generated structures and rare wave-ripple marks indicative of reworking by wave action, as common in mouth-bar deposits. Cross-bedded clean sandstones are interpreted to represent deposition from unidirectional tractive currents and are more typical of proximal mouth-bar deposits. Thinly bedded parallel-laminated clayey siltstones and siltstones deposited by suspension plumes and low-density turbidity currents are typical of distal mouth-bar deposits. Coarsening-upward pattern indicates mouth bar progradation; top truncation by coarse-grained channel fills (symmetrical log motif in wireline log signature) may record the propagation of distributary channels.	
Axial finer-grained delta	Distributary channel	up to 10 m	St, Sp, Srw, Src, Sm, Sc	Siltstones to fine-grained sandstones with well sorted and well rounded grains. Abundant massive structures, cm- to dm- scale trough cross-stratifications, planar-tabular cross-stratifications and current and wave-ripple laminations (facies St, Sp, Srw, Src, Sm and Sc in Table 2; Fig. 7). The basal surfaces are erosional and overlain by abundant intraformational mudstones or siltstones (mudstone rip-up clasts) and plant debris. Occasionally small-scale flutes and tool marks are present on the basal surface. This FA typically fines upward into siltstones or silty claystones. In places, the FA displays several stacked fining-upward vertical successions with or without internal erosional surfaces.	Typically overlies erosively fine-grained delta-plain deposits and/or prodelta deposits or mouth bar deposits. Overlain by fine-grained delta-plain deposits (leached palaeosols).	Bell-shaped, barrel-shaped or serrated bell-shaped, barrel-shaped log motifs starting at channel base. GR values increase upward (60-110 API).	This FA is typically deposited by tractive currents. Erosionally based sandstones with basal lags that fine upward through cross-bedded sandstones into ripple-laminated finer-grained sandstones with silt and clay alternations and association with fine-grained delta-plain deposits are typical features of active distributary channels (Bhattacharya and Walker, 1991; Olariu and Bhattacharya, 2006). The cross-bedding and current ripple lamination are interpreted to be the product of migration of dunes or ripple forms driven by unidirectional tractional currents under lower flow regime (Allen, 1982, 1985). The influence of tractive currents is further evidenced by occasional flutes and tool marks on basal surfaces. Upward fining is consistent with waning flow and possibly channel-fill abandonment. Erosional surfaces result from possible river-stage fluctuations or reworking by mobile channels.	Low to medium amplitude, moderate continuity, low-angle to flat-lying reflections. No apparent clinoformal shape.
	Interdistributary bay/swamp	< 5 m	Fl, Fc	Dark-grey or black organic rich parallel-laminated carboniferous claystones and silty claystones (facies Fc and Fl in Table 2) up to 5 m. Occasionally interlaminated dark-grey mudstones and muddy siltstones with rare current and wave ripples (facies Fl in Table 2) can be observed. Successions might coarsen or fine upwards. Thin coal beds, plant debris and pyrite nodules (Fig. 7B) are common.	Interbeds with relatively coarser-grained distributary-channel deposits.	Serrated log motif. High GR values (110 API).	This FA is interpreted to represent suspension fall-out in a low-energy interdistributary bay environment, with floods generating tractive current. Black and dark-grey organic-rich parallel-laminated fine-grained facies reflect suspension fall-out in anoxic bottom. The presence of thin coal beds, plant debris and pyrite nodules support a reducing environment. Occasional thin siltstone beds with rare current and wave ripples may record deposition from tractive currents in crevasse channels and crevasse splays into backswamp areas. An association with coarser-grained distributary channel fills suggests deposition in an interdistributary-bay and swamp environment.	
	Mouth bar	1 to 5 m	St, Sp, Shl, Src, Srw	Predominantly clean siltstones (quartz arenites) with well-sorted and well-rounded grains. Common coarsening-upward patterns from thinly bedded parallel-laminated and current-ripple laminated clayey siltstones and siltstones to cross-stratified or massive clean light-yellow very fine-grained sandstones	Typically overlies fine-grained delta-front or prodelta deposits gradationally.	Funnel-shaped or serrated funnel-shaped log motif	This FA is characterized by clean sandstones/siltstones of high compositional and textural maturity with dominant traction-generated structures and rare wave-ripple marks indicative of reworking by wave action, as common in mouth-bar deposits (e.g. Bhattacharya and Walker, 1991;	

				or siltstones (St, Sp, Shl, Src, Srw and Fl in Table 2; Fig. 7A). In some cases, symmetric ripple marks are present.	Overlain by coarser-grained cross-bedded or massive sandstones of distributary-channel or crevasse-channel origin or by fine-grained delta-plain deposits.	while in places, it forms the lower part of the symmetrical log motif. GR values start at ca. 110 API at the base of the log facies whereby the GR curve might be serrated and cleans upward to ca. 60 API.	Bhattacharya, 2006; Wellner et al., 2006). Cross-bedded clean sandstones are interpreted to represent deposition from unidirectional tractive currents and are more typical of proximal mouth-bar deposits (Bhattacharya and Walker, 1991; Olariu and Bhattacharya, 2006). Thinly bedded parallel-laminated clayey siltstones and siltstones deposited by suspension plumes and low-density turbidity currents are typical of distal mouth-bar environments (Bhattacharya and Walker, 1991; Olariu and Bhattacharya, 2006). Coarsening-upward pattern indicates mouth-bar progradation; top truncation by coarse-grained channel fills (symmetrical log motif in wireline log signature) may record the propagation of distributary channels.	
	Delta-front	up to 10 m	Fl, Shl, Sd, Sm, Sg	Predominantly alternating siltstone and mudstone layers and thin very fine sandstone interbeds (Fl, Shl, Sd, Sm and Sg in Table 2). The sandstone units commonly occur as massive, sharply or erosively based channelized very fine sandstones/siltstones or sheet-like massive very fine sandstones/siltstones (typically < 1 m). In places, abundant soft-sediment deformation such as load casts and flame structures, dewatering structures and convolute laminations are present near the basal contact.	Commonly overlies prodelta parallel-laminated dark-grey mudstones and siltstones. Overlain by mouth bar deposits, either gradationally or with erosional contact.	Serrated funnel-shaped log motif. GR values around 120 API.	This FA is interpreted to represent delta-front deposits accumulated beyond distributary mouth bars of the advancing river deltas (Olariu and Bhattacharya, 2006; Schomacker et al., 2010). Fine-grained mudstones and muddy siltstones were deposited by suspension by hypopycnal or homopycnal flows. Thin channelized or sheet-like very-fine sandstone beds may reflect deposition of confined or unconfined density currents overpassing mouth bars during river floods (hyperpycnal flow) (Mulder et al., 2001; Mulder et al., 2003). Abundant soft-sediment failure suggests post-depositional processes, indicating rapid deposition or loading by landslides or waves (Sabato, 2007; Bridge and Demicco, 2008), which might result from delta collapse due to gravitational instability of the deltas.	
	Wave-dominated (or -influenced) nearshore	0.5 to 10 m	Srw, Sl	Very fine- to fine-grained sandstones and siltstones (well sorted, well rounded grains) with abundant wave-ripple cross laminations and subordinate parallel laminations (Srw and Sl in Table 2; Fig. 8). Occasionally intercalations of clayey siltstones with brackish fauna can be observed. Grain-size distribution is dominated by suspended-load deposits (>80%; Fig. 8D). Present at locations WL, PC and WC in the northern-central part of the basin.	Commonly underlain gradationally and overlain sharply by lacustrine dark-grey or black mudstones. Locally overlain by cross-bedded distributary-channel sandstones.	Clean funnel-shaped log motif. GR values change from 5 to 10 API upwards (Fig. 8A). Low GR values possibly due to the proximity with salt layers.	This FA is dominated by very fine-grained sandstones/siltstones with high textural maturity, shows abundant bidirectional wave-ripple laminations, and occurs in association with lacustrine black or dark-grey mudstones; these features make this FA interpretable as wave-dominated or wave-influenced nearshore deposits (Renaut and Owen, 1991; Bray and Carter, 1992; Keighley, 2008). Degree of textural maturity and abundant bidirectional wave-ripple marks are typical of wave reworking above the mean fairweather wave base (Allen, 1979, 1981).	
	Prodelta	Up to 5 m.	Fc, Fl, Sd, Sg	Parallel-laminated dark-grey mudstones and fine-grained siltstones or massive dark-grey mudstones (Fl, Fc, Sd and Sg in Table 2), typically upward coarsening. In some cases, bioturbations can be observed. Occasionally thinly-bedded sharp-based graded very fine-grained sandstones or siltstones are present. Locally abundant in soft-sediment deformation.	Typically overlies dark-grey mudstones of open-lake deposits. Overlain by delta-front deposits, mouth-bar deposits and wave-dominated nearshore deposits.	Serrated or serrated funnel-shaped log motif. GR values around 120 API.	This FA is interpreted to be prodelta deposits accumulated by suspension fall-out from hypopycnal or homopycnal flows and by intermittent deposition by flood-generated hyperpycnal flows (Mulder et al., 2001; Mulder et al., 2003; Olariu and Bhattacharya, 2006).	
Open lake	Lacustrine mudstones	Typically 10 m, ranging from 1 to 30 m.	Fc, Fl, Fr	Predominantly parallel-laminated or massive, dark-grey and black claystone and silty claystone. Occasionally reddish or purple coloured and rare desiccation cracks.	Typically overlain by prodelta parallel-laminated siltstone and mudstone or mouth-bar siltstone deposits. Also interbedded with evaporitic deposits.	Serrated or straight log motif with a variable GR value (salt containment dependent).	This FA is interpreted to be low-energy open-lake deposits formed by suspension fall-out under stagnant anoxic bottom conditions (Demaison and Moore, 1980; Scholz et al., 2011), which may have been favoured by a stratified water column, as commonly seen in lacustrine environments (Halfman, 1993). Rare reddish or purple coloured mudstones and desiccation cracks may indicate periodic emergence (Allen, 1985).	Medium to high amplitude, moderate to high continuity, sub-parallel to parallel reflections that are relatively flat-lying to gently dipping (commonly draping the underlying topography).
	Evaporitic saline-lake deposits	Up to 600 m	Hg	Thick salt layers, gypsum layers, gypsiferous salt and gypsiferous mudstone with rare pyrite and plant debris (facies Hg in Table 2; Fig. 9). Typically vertical successions change upwards from interbedded sandstones and dark-grey mudstones, gypsiferous mudstones, gypsum beds, salt beds, gypsum beds, gypsiferous mudstones to dark-grey mudstones.	Commonly interbedded with open-lake dark-grey or black mudstone.	Very low GR values (3-5 API), low bulk density values (around 2.04-2.35 gm/cc) and high resistivity (30-40 $\Omega \cdot m$) (Fig. 9A).	This FA is interpreted as having been formed in a deep perennial saline lake environment during lake regression (Sirota et al., 2018), or as the product of lake desiccation due to evaporation within an arid climatic setting through deposition at the basin centre during phases of lake regression that were possibly climate-driven (Ji et al., 2005a).	High amplitude, high continuity, sub-parallel to parallel reflections that are relatively flat-lying to gently dipping (commonly draping the underlying topography).
	Gravity-flow-dominated lake bottom	3 to 20 m	Gm, Sm, Sg (St, Sp, Src), Sd	Mainly chaotic, poorly sorted matrix-supported pebble-grade massive conglomerates (⌀ <5cm) or fine to coarse sandstones. Occasionally fining upward successions from massive conglomerates or gravelly sandstones (occasionally normal graded), crude cross-laminated sandstones to fine sandstones. Basal contacts are sharp, with erosional or non-erosional relief. At the bed bases, abundant rip-up clasts and soft-sediment deformation such as load casts, dewatering and convolute laminations and sand injections.	Often sharp or erosional, basal contact, and irregular or undulated upper contact, with lacustrine dark-grey or black mudstone.	Highly erratic.	The clast size and chaotic, poorly sorted, matrix-supported nature, the loaded basal contacts and the association with lacustrine mudstones make this FA interpretable as gravity-flow-dominated deposits in an open-lake environment. Matrix-supported conglomerates suggest rapid deposition from debris flows (Lowe, 1982; Surlyk, 1984). Fine to coarse sandstones may represent remobilized beds of sandstone in the mass transport deposits, preserved in slides or slumps. The fining-upward successions from graded sandstones, cross-laminated sandstones to fine sandstones may indicate deposition of high-density turbidity flows (Allen, 1985), representing Bouma sequence (cf. Bouma, 1962). The poor sorting, clast size and presence of intraformational rip-up clasts implies limited transport distance of the sediments from the original sources. The deposits of this FA are possibly associated with delta-slope collapse due to gravitational instability driven in part by seismicity of the adjacent faults.	Below seismic resolution

4.1.1 Footwall-derived coarse-grained fan delta

The deposits assigned to this type of deltaic systems sit directly atop the hangingwall of the main basin-bounding fault (Lanliao Fault) at the eastern edge of the basin. They are typically restricted to a narrow fringe (<5 km in dip length; <9 km in strike width) adjacent to the boundary fault. Five footwall-derived fan-delta systems located in MG, QLY, BM, DZ and XZ can be recognized in the DPD. Imaging of these clastic bodies through seismic data demonstrates medium seismic amplitude, moderate continuity, steep-dipping reflections (ca. 30°) and continuous to chaotic internal reflections. In seismic data, they either exhibit a 3D prism-apron shape parallel to the fault plane or progradational clinoforms dipping away from the fault. In planview, clastic bodies associated with individual deltas of this type exhibit a radial distribution of elongated, sharp-based, channelized sandbodies, which emanate from a point source in the footwall (see section 4.3).

Deposits in this type of depositional environment mainly comprise coarse-grained, poorly sorted, conglomerates with angular to subangular grains, gravelly sandstones, sandstones, and interbedded sandstones and mudstones (Fig. 5). In the available cores, only stream-dominated topset deposits could be identified; no core data are available from intervals that correspond to fan delta foresets and toesets imaged in the seismic data. Therefore, only FAs associated with fluvial delta topsets including alluvial channel-fill and delta-plain deposits (Fig. 5) could be described and interpreted in detail (Supporting Information 1 and Table 3).

4.1.2 Footwall-derived sand-rich delta

The deposits assigned to this type of deltaic system occur mainly at locations HZJ and QZJ, where they accumulated on top of the hangingwall of the main basin-bounding fault (Shijaji Fault), at the northwest edge of the basin. In the seismic data, this delta type exhibits medium seismic amplitude, discontinuous, dipping reflections that are separated by high amplitude, flat-lying reflections. The dipping reflections display a low-angle (ca. 5°-10°), basinward-dipping clinoform geometry. The foresets are arranged into sets that display a highly progradational stacking pattern. In seismic data, these units commonly exhibit a 3D radial geometry and are predominantly positioned in the immediate hangingwall of the border fault. Sand-rich packages of this type of depositional environment are typically fine- to coarse-grained sandstones, which are overall finer than those forming the footwall-derived fan deltas and coarser than those forming the axial fine-grained deltas. In the available cores, FAs relating to distributary channels, interdistributary bays or swamps and mouth bars could be recognized in this type of deltaic units (Fig. 6), as detailed in Supporting Information 1 and Table 3.

4.1.3 Axial finer-grained delta

The deposits assigned to this type of deltaic systems are mainly concentrated along the axial areas centred on the Central Uplift in the south and north of the study area. The seismic expression of this delta type is characterized by low to medium seismic amplitude, moderate continuity, low-angle to flat-lying reflections (ca. 0°-5°); these deposits typically exhibit no apparent clinoform shape in seismic profiles but in places, progradational stacking patterns of clinoforms (ca. 0°-5°) can be recognized. The deposits are typically of siltstone to fine-grained sandstone with well-sorted and well to moderately rounded grains. Six FAs could be recognized in association with this type of delta in cores, representing distributary-channel, interdistributary-bay or -swamp, mouth-bar, delta-front, wave-dominated/influenced nearshore and prodelta subenvironments (Figs. 7 and 8), as detailed in Supporting Information 1 and Table 3.

4.1.4 Open lacustrine deposits

4.1.4.1 Open-lacustrine mudstones

The deposits of this FA are mainly encountered along the palaeo-depressions of the Eastern and Western troughs, where they appear as parallel-laminated or massive, black to dark-grey claystones and silty claystones that are up to 30 m thick (facies Fc and Fl in Table 2). Rarely, reddish or purple coloured deposits and desiccation cracks can be present. The deposits of this FA are typically overlain by prodelta parallel-laminated siltstone and mudstone or mouth-bar siltstone deposits; in places these are interbedded with evaporitic saline-lake deposits. In the seismic data, these units demonstrate medium- to high-amplitude, moderate- to high-continuity, sub-parallel to parallel reflections that are relatively flat-lying to gently-dipping, and which commonly drape the underlying topography. The GR logs display a serrated or straight log motif, with variable GR values depending on salt content. These

massive black to dark-grey mudstones are interpreted to be low-energy open-lake deposits formed by suspension fall-out in stagnant anoxic bottom conditions. A stratified water column, which is commonly seen in deep lacustrine environment, may have favoured such stagnant bottom conditions (Halfman, 1993). For instance, in the modern Lake Malawi, permanent stratification exists, whereby water mixing only develops above depths of 250 m, below which the lake is in permanently anoxic conditions (Halfman, 1993). Rare reddish or purple mudstones and desiccation cracks may indicate periodic emergence (Allen, 1985).

4.1.4.2 Evaporitic saline-lake deposits

The deposits of this FA comprise thick salt layers, gypsum layers, gypsiferous salts and gypsiferous mudstones with rare pyrite and plant debris (facies Hg in Table 2) (Fig. 9). In this FA, halite dominates and is present as thin to thick discrete beds, and small disseminated crystals or nodules encased in open-lacustrine dark grey mudstone, in a colourless to light-yellow colour. They are best exposed in cores at locations WL and HBZ in the northern-central part of the basin, covering an area of ca. 420 km^2, with the largest cumulative thickness of ca. 600 m penetrated by PS7 for the ES_3 interval. The deposits of this FA mainly exist in the central deep parts of the basin or atop the hanging wall of faults and are missing from the shallow marginal parts. They are commonly interbedded with open-lake dark-grey or black mudstones. In the seismic data, these deposits exhibit high-amplitude, high-continuity, sub-parallel to parallel reflections that are apparently flat-lying or gently-dipping, and which commonly drape the underlying topography. Wireline logs show very low GR responses (3-5 API), low bulk density values (ca. 2.04-2.35 gm/cc) and high resistivity (30-40 $\Omega \cdot m$) (Fig. 9A). The deposits of this FA are interpreted as either having formed in a deep perennial saline lake environment during lake regression (Sirota et al., 2018; cf. Tänavsuu-Milkeviciene and Sarg, 2012; Roveri et al., 2014; Kiro et al., 2017), or as the product of lake desiccation due to evaporation in an arid climatic setting (Nadon and Middleton, 1985), whereby deposition takes place at the basin centre during phases of lake regression that may be driven by climatic changes (Ji et al., 2005a).

4.1.4.3 Gravity-flow-dominated lake-bottom deposits

The deposits of this FA are mainly ponded in the hangingwalls immediately adjacent to intrabasinal faults due to frontal confinement; one such example is the Duzhai Fault at location BM in the Eastern Trough and the Changyuan Fault at locations HZJ and QZJ in the Western Trough (see section 5.3). In core, these deposits appear as chaotic, poorly sorted matrix-supported pebble-grade massive conglomerates ($\varnothing_{max}$ <5 cm) or fine to coarse sandstones with a thickness of 3-20 m. The wireline log signature is notably erratic. These deposits are below seismic resolution. In a few places, the internal facies patterns of lacustrine gravity-flow deposits record an overall fining-upward succession that transitions from massive conglomerates or gravelly sandstones (occasionally normally graded), through crude cross-laminated sandstones to fine sandstones (facies Gm, Sm, Sg and Sd in Table 2). Abundant intraformational mudstone rip-up clasts and soft-sediment deformation such as load casts, dewatering, convolute laminations and sand injections, can be observed near the bases of beds. Typically, lacustrine gravity-flow deposits exhibit a sharp, commonly erosional, base, and irregular or undulated top, and are encased in thick lacustrine dark-grey or black mudstones.

The features are typical of gravity-flow-dominated deposits in an open-lake environment. Matrix-supported conglomerates suggest rapid deposition from debris flows (Lowe, 1982; Surlyk, 1984). Fine to coarse sandstones may represent remobilized beds of sandstone in the mass transport deposits, preserved in slides or slumps. The fining-upward successions from graded sandstones, cross-laminated sandstones to fine sandstones may indicate deposition of high-density turbidity flows (Allen, 1985), representing Bouma sequence (cf. Bouma, 1962). The poor sorting, clast size and presence of intraformational rip-up clasts implies limited transport distance of the sediments from the original sources. The association of this FA with thick lacustrine dark-grey or black mudstone suggests deposition in an open-lacustrine environment. Lacustrine gravity-flow deposits are possibly associated with delta-slope collapse due to gravitational instability driven in part by seismicity of the adjacent faults.

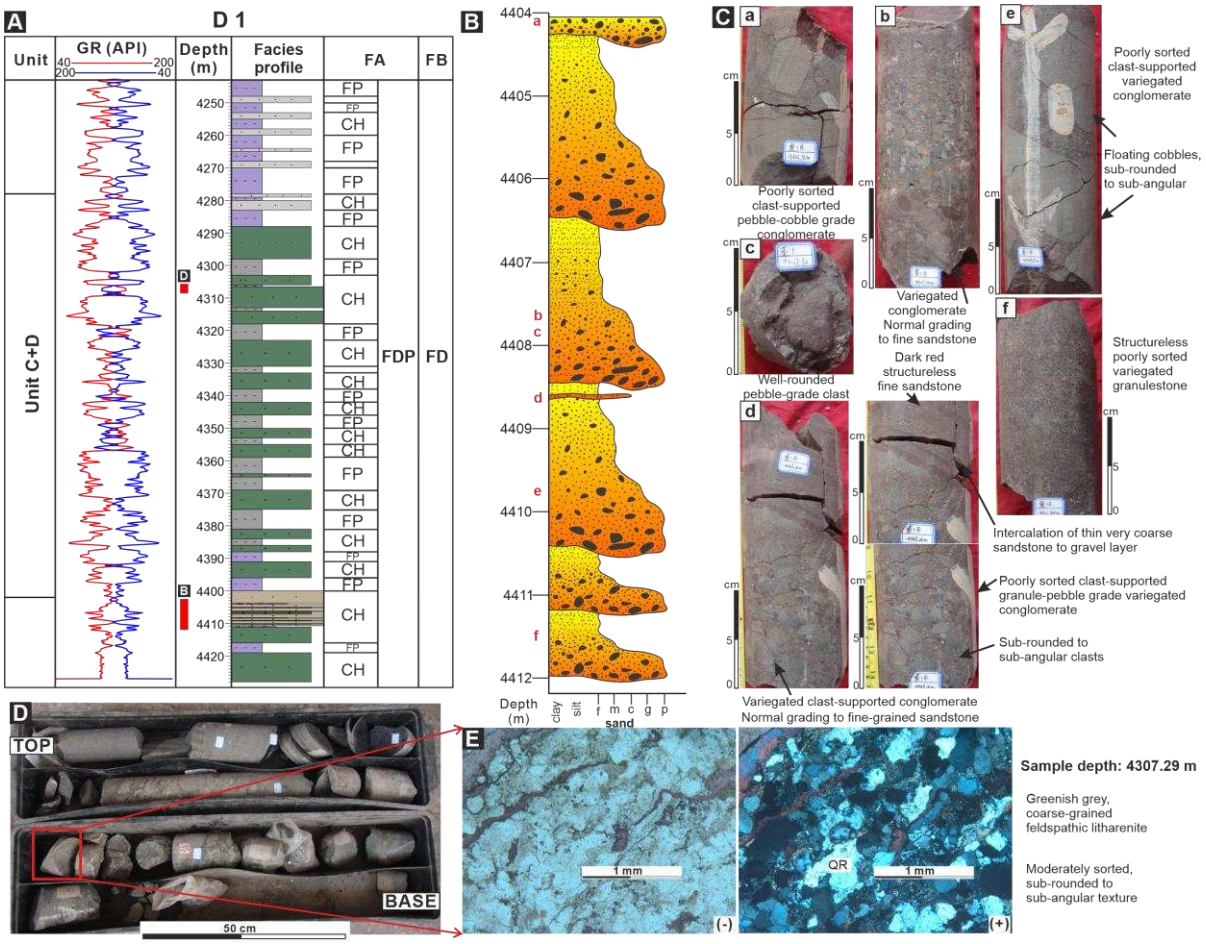

Fig. 5. Sedimentological characteristics and wireline-log signatures of facies associations (alluvial channel fill and delta-plain topset) of a footwall-derived coarse-grained delta in well D1. Since only alluvial topsets could be identified in the available cores, only deposits associated with alluvial topsets are shown. (A) Wireline log and associated grainsize profile from well cuttings. Red bars denote the cored intervals in well D1, which are illustrated in B and D, respectively. See Figure 2 for legend. (B-C) Sedimentary log and core photos for an alluvial channel fill of variant B. (D-E) Core photos (D) and thin-section photos (E) for an alluvial channel fill of variant A. The photos in E are for the same thin section under parallel (-) and crossed polars (+). CH = alluvial channel fill; FP = delta-plain alluvial topset; FA = facies association; QR = quartz.

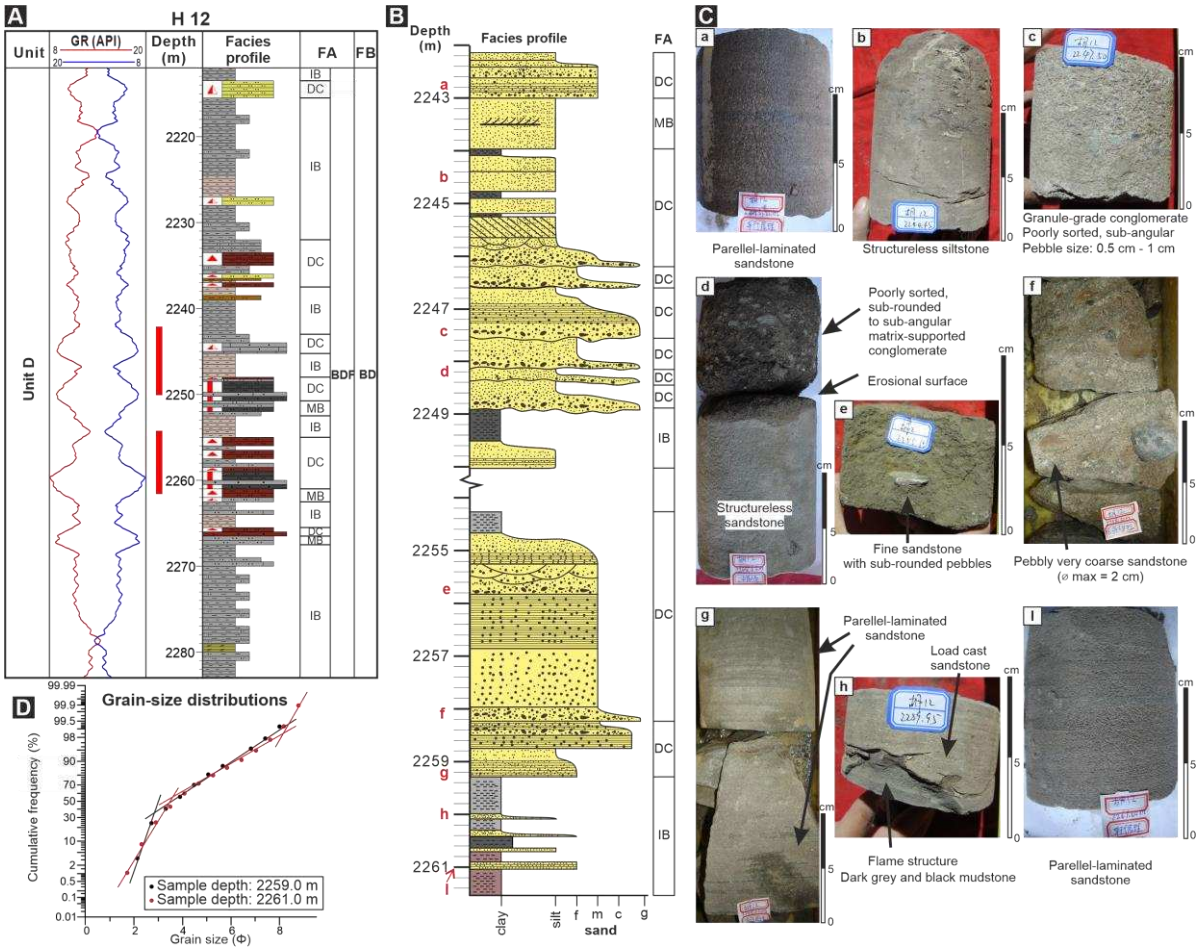

Fig. 6. Sedimentological characteristics and wireline-log signatures of facies associations of a footwall-derived sand-rich delta in well H12. (A) Wireline log and grainsize profile from well cuttings. Red bars denote the cored intervals in well H12, which are illustrated in B. See Figure 2 for legend. (B-C) Sedimentary log and core photos of facies associations. (D) Grain-size distributions for samples in well H12 (2259 m and 2261 m). DC = distributary-channel fill; IB = interdistributary bay/swamp; MB = Mouth bar; FA = facies association.

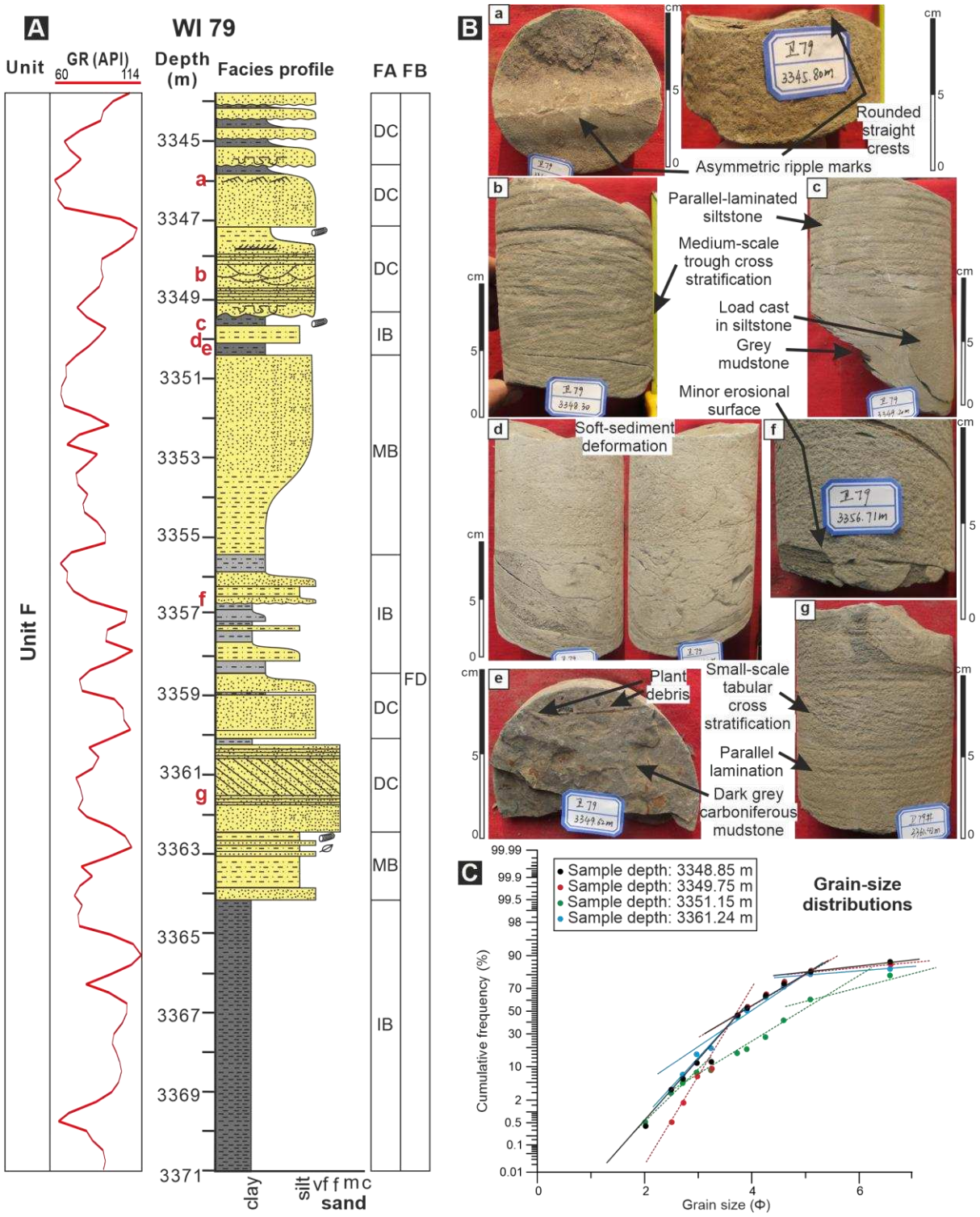

Fig. 7. Sedimentological characteristics and wireline-log signatures of facies associations of an axial fine-grained delta in well WI79. (A) Wireline log and sedimentary log for facies associations defined by analysis of cored intervals. (B) Core photos for specific facies associations shown in A. (C) Grain-size distributions for samples in well WI79 (3348.85 m, 3349.75 m, 3351.15 m and 3361.24 m). DC = distributary channel; IB = interdistributary bay or swamp; MB = mouth bar; FA = facies association.

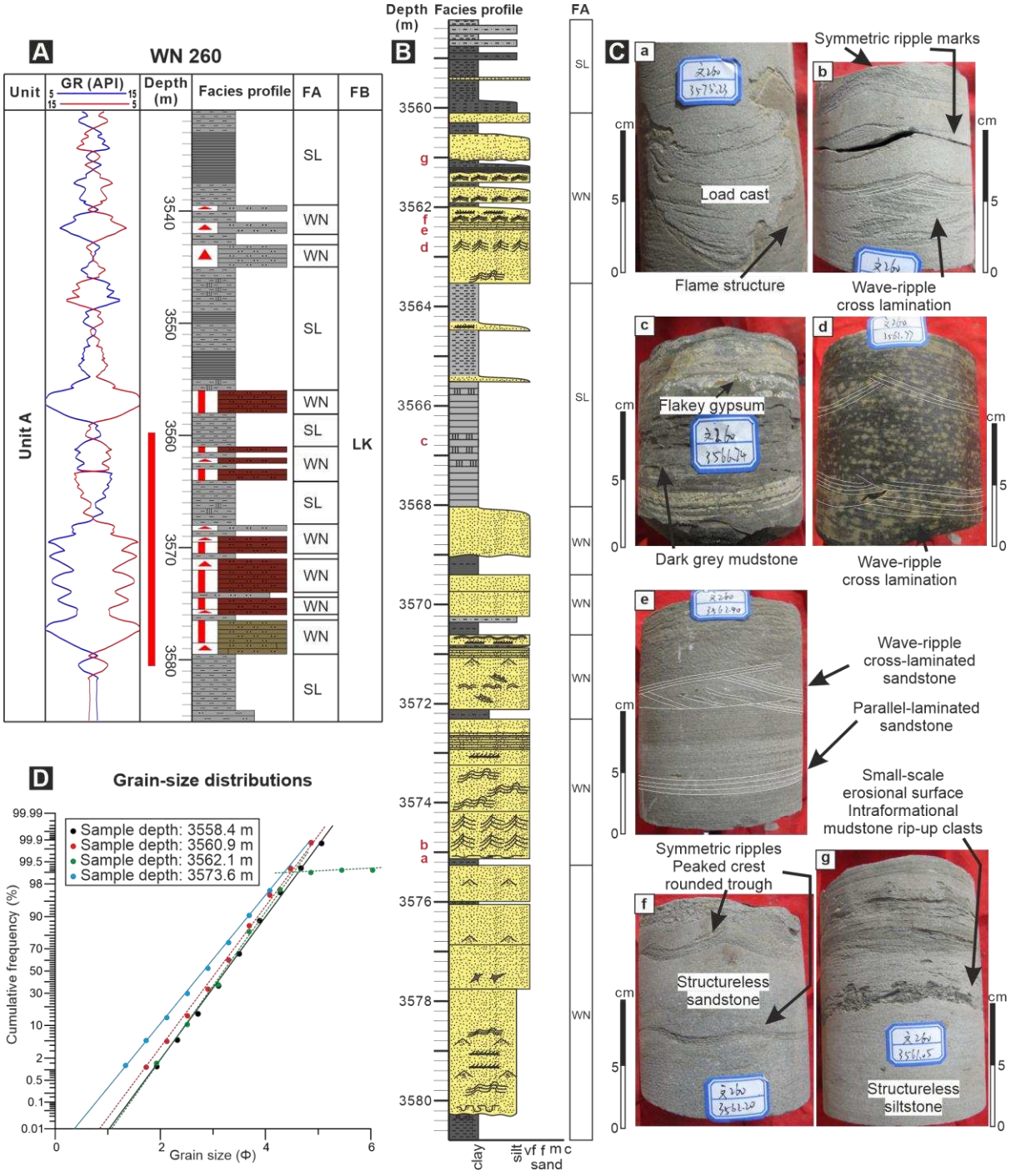

Fig. 8. Sedimentological characteristics and wireline-log signatures for wave-dominated (or -influenced) nearshore deposits and open-lacustrine deposits in well WN260. (A) Wireline log and grainsize profile from well cuttings. The red bar denotes the cored interval in well WN260, which is illustrated in B. See Figure 2 for legend. (B-C) Sedimentary log and core photos for given FAs. (D) Grain-size distributions for samples in well WN260 (3558.4 m, 3560.9 m, 3562.1 m and 3573.6 m). WN = wave-dominated (or -influenced) nearshore deposits; LK = lacustrine deposits; FA = facies association.

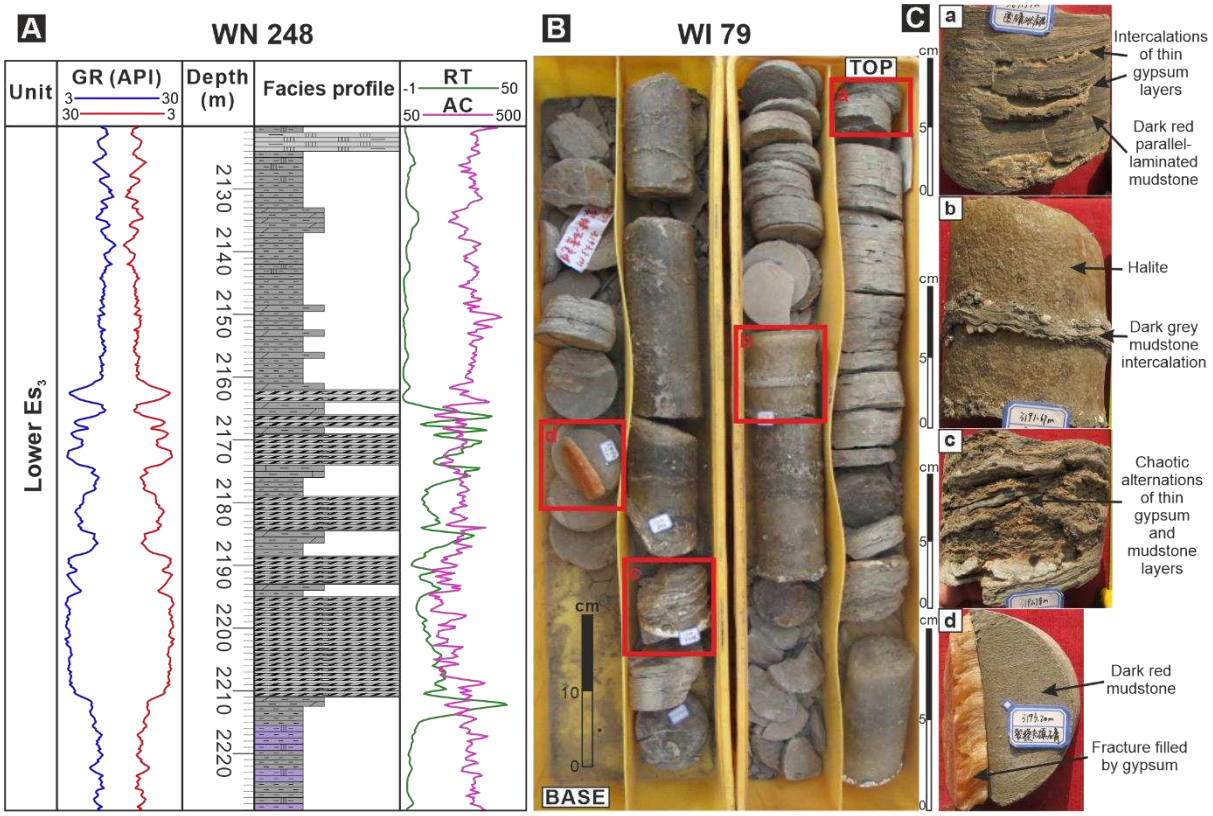

Fig. 9. Sedimentological details and wireline-log signatures for evaporitic saline-lake deposits. (A) Wireline log and grainsize profile based on cuttings from well WN248. See Figure 2 for legend. (B-C) Representative core photos for evaporitic deposits from well WI79.

4.2 Sandstone petrography and heavy minerals

A petrographic analysis of 165 thin sections taken from sandstone or siltstone samples from the cored wells in the DPD stratigraphy is undertaken using a standard transmitted light petrological microscope. This analysis is supplemented with petrographic data obtained from unpublished well reports for 114 wells, which have been cross-checked for methodology and consistency. Compositional data obtained for sandstones or siltstones of the DPD stratigraphic units (Lower Es_3, Middle Es_3 and Upper Es_3) are shown in Figs. 10-12. Values of maturity index, i.e., the ratio of quartz fraction relative to the sum of feldspar and lithic fragments, is also indicated for the studied examples and shown in Fig. 10 as contours. No significant variation has been noted in the proportions of the main detrital components (quartz, feldspar, sedimentary, metamorphic and volcanic lithic fragments) between the different stratigraphic units, though some modest variability is observed. Overall, the sandstones or siltstones in the Es_3 interval of the DPD are dominantly of subarkose, sublitharenite to arkosic arenite composition (Fig. 11A). Here, we focus on the Middle Es_3 section. Sandstone composition in the north of the DPD (locations WMZ, MZ, PC and WC) is dominated by subarkose and subordinate lithic arkose, with a southward increase of maturity index from 1.25 to 4.66; the lithics are generally characterized by a mixing of sedimentary, volcanic and metamorphic fragments. The sandstones along the northwestern edge of the basin (locations HZJ and QZJ) are predominantly litharenite to feldspathic litharenite, with average maturity index of 1.51; lithic fragments are mainly composed of sedimentary lithics (average ca. 50%-60% of total lithics), subordinate metamorphic lithics (average ca. 30%-45% of total lithics) and low to absent volcanic lithics. In the southwestern areas of the basin, only two boreholes (PS8 and S2) are available for petrographic analysis. Samples from both wells contain a significant proportion of volcanic lithics (ca. 45% and 70% of all lithics, respectively). The sandstones in the central part of the basin (location QK) are dominated by lithic arkose and subordinate subarkose with an average maturity index of 2.46; the lithics are dominated by sedimentary and metamorphic fragments, with an increase in the volcanic lithic content to the south and east of this area. The sandstone samples in the southeast of the basin (locations ZY, SCJ and XJ) are predominantly lithic arkose to arkose, with an average

maturity index of 1.58; sedimentary, volcanic and metamorphic lithic fragments are all present in these samples, but a decrease in the proportion of volcanic lithics and an increase in the proportion of metamorphic lithics is noted moving northward. For samples in the hangingwall of the Lanliao Fault system, sandstones are predominantly litharenite to feldspathic litharenite, with an average maturity index of 1.58; here, the lithics are composed of abundant sedimentary lithic fragments (max. 70%) and subordinate metamorphic lithic fragments (max. 50%).

Data on heavy-mineral assemblages of the studied intervals are compiled from unpublished company reports and are shown in Fig. 14. The ZTR index (sum of zircon, tourmaline and rutile over total transparent heavy minerals) is utilized to assess the compositional maturity of deposits sampled across the basin and throughout the stratigraphy (Hubert, 1962). Samples for the three studied intervals (Lower Es_3, Middle Es_3 and Upper Es_3) are respectively taken from 44, 85 and 24 wells (Fig. 14). No systematic change is noted in the spatial distribution of the heavy-mineral assemblages across the different stratigraphic units. Here, we focus on the Middle Es_3 section. Heavy-mineral assemblages in the north of the basin (locations WMZ, PC and WC) are dominated by zircon (20-72%), garnet (30%-45%) and tourmaline (10-20%), with predominantly high ZTR values (>0.6). Samples along the northwestern edge of the basin (locations HZJ and QZJ) are dominated by garnet (max. 82%), perovskite (max. 50%) and magnetite (max. 30%), with predominantly mid-range ZTR values (0.4-0.5). The assemblages in the central part of the basin (locations FLJ, QK and MJ) are dominated by zircon (max. 60%), tourmaline (15%-20%) and garnet (max. 20%) with anomalously high proportions of perovskite or chloritoid in certain samples. Here, the ZTR is predominantly high (> 0.6) with very high values noted for samples at location QK (0.80-0.95). In the southeast of the basin (locations SCJ, MC and ZY), the samples are notably abundant in garnet (max. 80%), with predominantly low ZTR values ranging from 0.16 to 0.41 northward. Along the hangingwall of the Lanliao Fault system, the assemblages are notably abundant in magnetite (30%-50%), with the exception of samples from location BM, which are dominated by zircon (39%-49%), tourmaline (17-26%) and magnetite (17%-20%). Along the eastern edge of the basin, the ZTR values are more variable, ranging from 0.46 to 0.85. In the central-northern part of the basin (location WL), the heavy-mineral assemblages are markedly more variable than those at other locations, with zircon fractions ranging between 20% and 50%. The ZTR values in this area are predominantly high, ranging from 0.63 to 0.94.

More detailed descriptions of sandstone petrography and heavy-mineral assemblages for all stratigraphic units (Lower Es_3, Middle Es_3 and Upper Es_3) are presented in the Supporting Information 2.

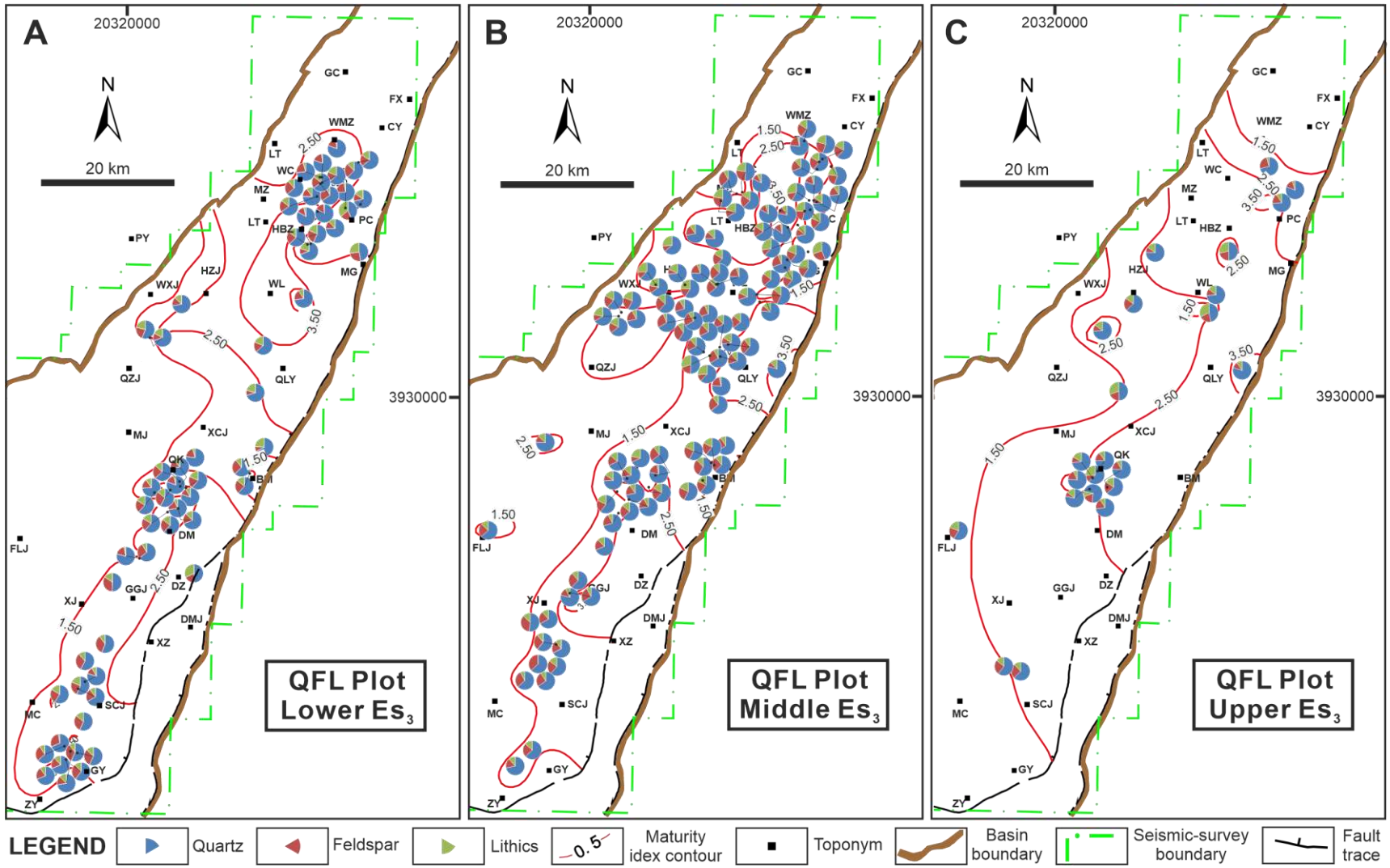

Fig. 10. Spatial distribution of compositional data for sandstones or siltstones across the DPD in the studied stratigraphic units (Lower Es_3, Middle Es_3 and Upper Es_3). Values of maturity index, i.e., the ratio of quartz to the sum of feldspar and lithic fragments, are shown in the maps as contours based on inverse-distance interpolation.

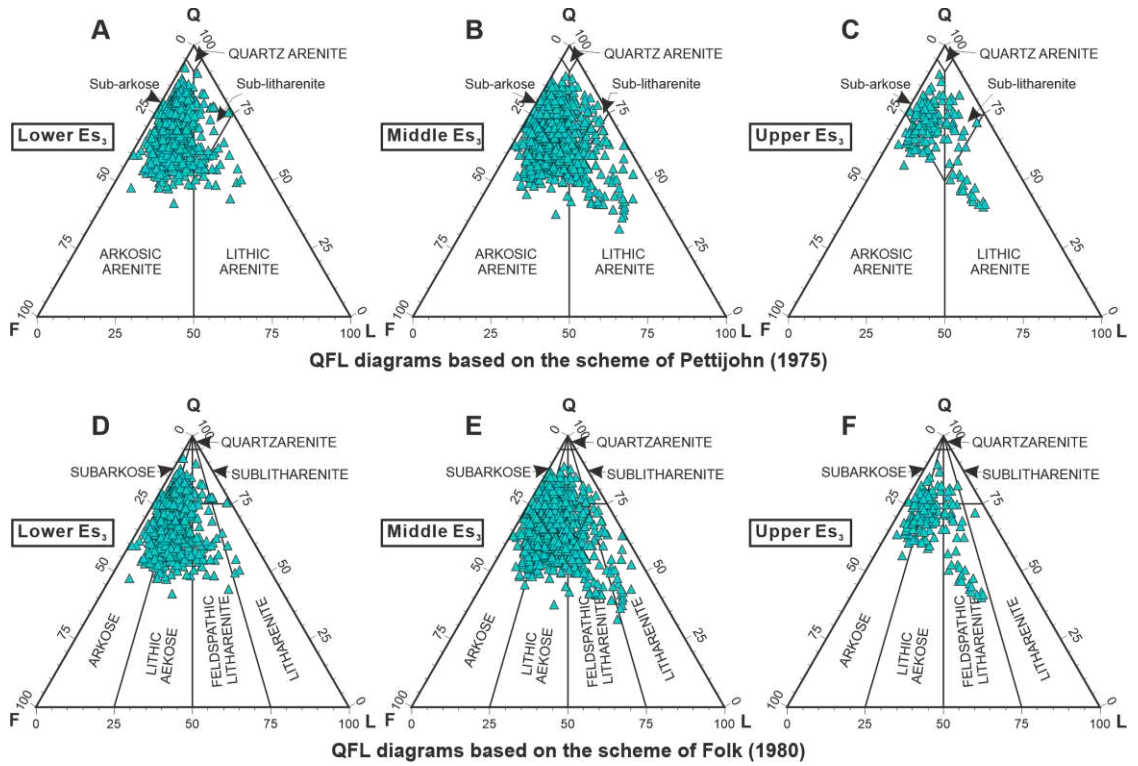

Fig. 11. Petrography of the sandstone or siltstone samples from the DPD stratigraphy (Lower Es_3, Middle Es_3 and Upper Es_3), with petrographic classes based on the schemes by (A-C) Pettijohn (1975) and (D-F) Folk (1980). Standard plots: Quartz, Feldspar, Lithic grains (Q, F, L), showing the subarkosic to sublitharenite nature of the sandstones and siltstones of the DPD stratigraphy.

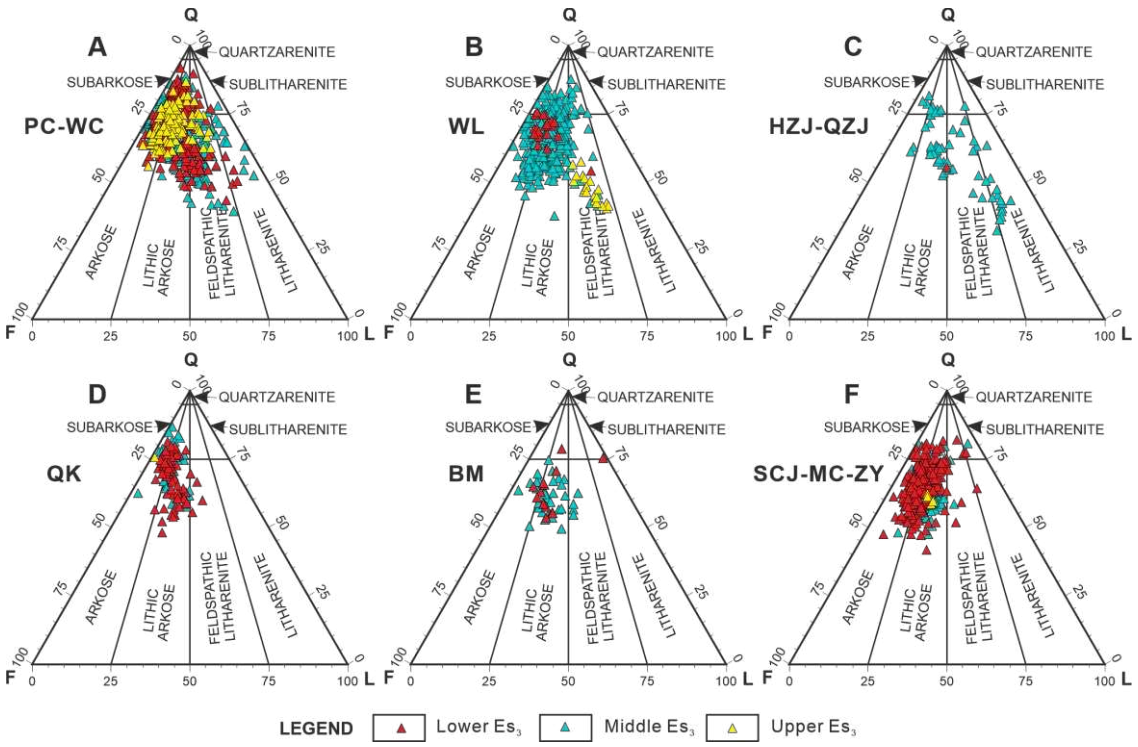

Fig. 12. Petrography of the sandstone or siltstone samples for different areas and stratigraphic intervals of the DPD fill, with petrographic classes based on the scheme by Folk (1980). Each diagram relates to a different area; data are colour-coded by stratigraphic interval. Q = Quartz; F = Feldspar; L = Lithic grains. See Figure 1 for location abbreviations.

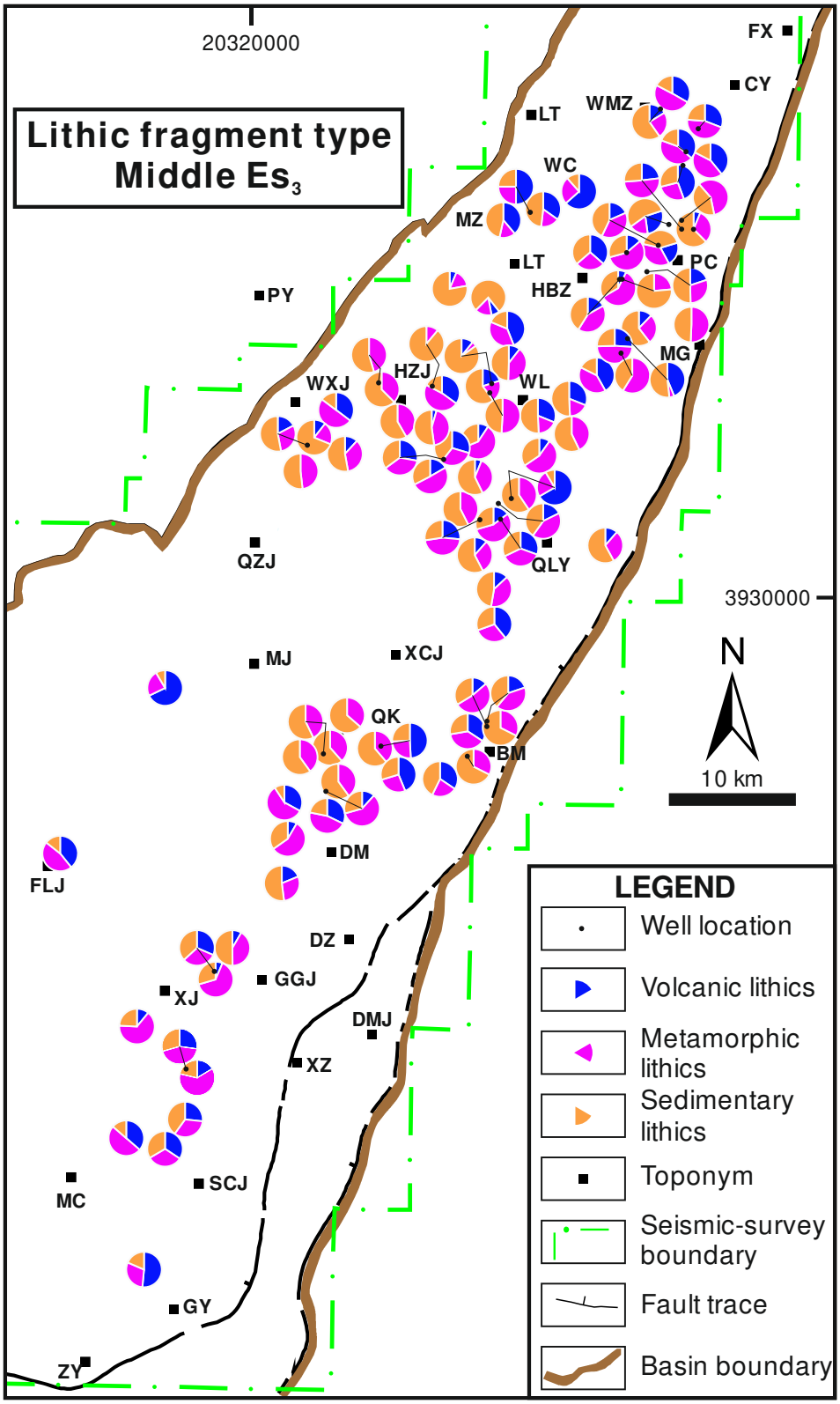

Fig. 13. Spatial distribution of lithic fragment types for sandstones or siltstones across the DPD in the study interval (Middle Es_3).

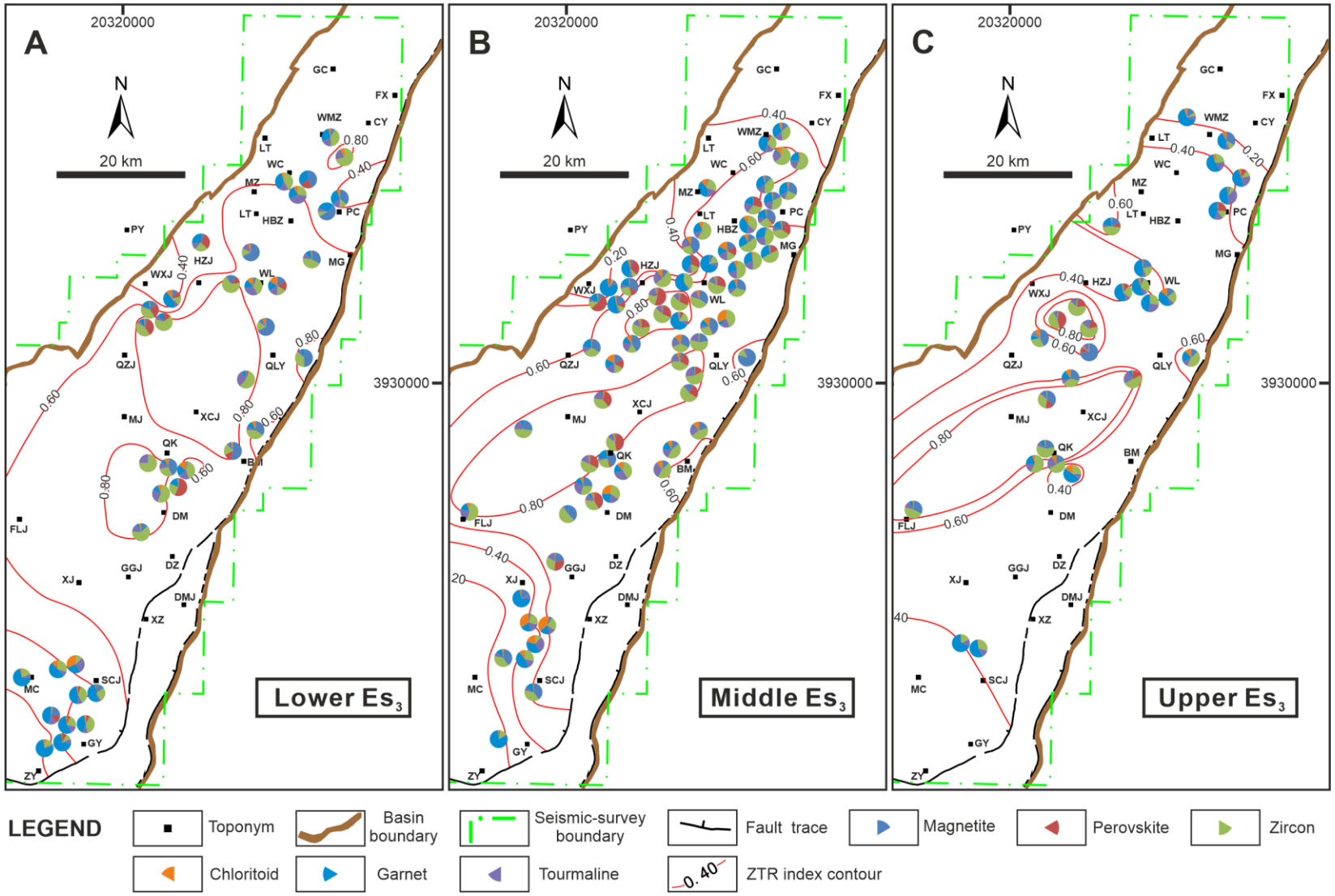

Fig. 14. Composition of the heavy-mineral assemblages for samples across the DPD for the different stratigraphic units (Lower Es_3, Middle Es_3 and Upper Es_3). Values of the ZTR index are shown in the maps as contours based on inverse-distance interpolation.

4.3 Seismic interpretation of depositional systems in the DPD

The overall thickness of the studied intervals (units A-F) is generally below the vertical resolution of the available seismic data. In order to better understand sandstone or siltstone thickness distributions and improve palaeogeographic reconstructions for regions of the DPD covered by sparse boreholes, such as locations FLJ, SCJ and part of the hangingwall of the Lanliao Fault (Fig. 3), interpretations of seismic geomorphology are undertaken for each study interval (units A-F) based on seismic-attribute maps. Two representative seismic-attribute maps of the studied interval covering the top of the hangingwall of the Lanliao Fault and location FLJ are presented in Figure 15. Interpretation of these attribute maps is calibrated by comparison with borehole analysis. Depth contours for the basement of the Lanliao Fault footwall in Figure 15A demonstrate the presence of several relatively deeply incised drainage outlets (*sensu* Chen et al., 2020) in the footwall of the Lanliao Fault. These basement depressions, which are interpreted as the preserved expression of bedrock-incised gorges that acted as feeder valleys, might have formed point-sources to two large fan deltas in the adjacent hangingwall of the Lanliao Fault, with the northern fan delta having a dip length of ca. 2 km and a strike width of ca. 4 km, and the southern one being ca. 4 km long and >4 km wide.

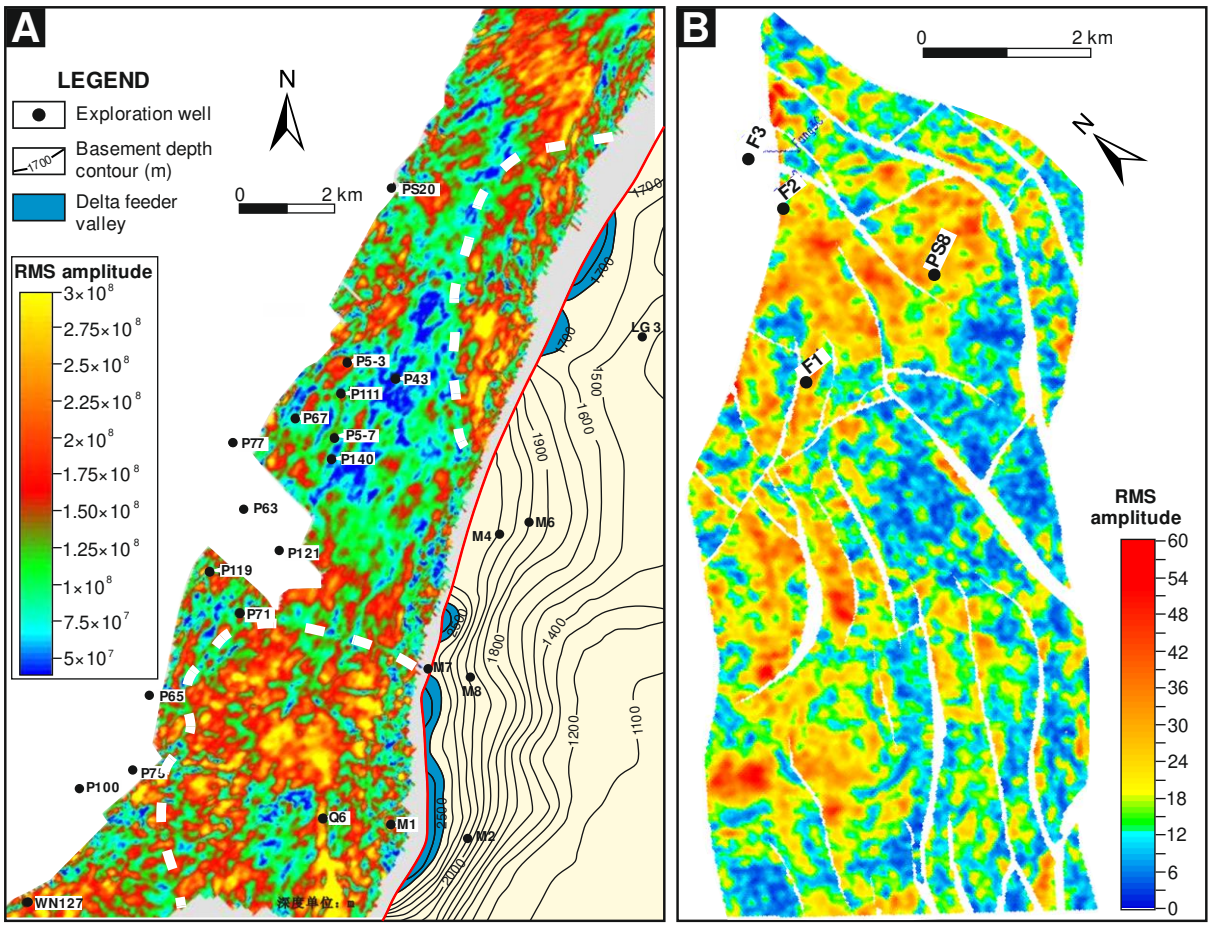

Fig. 15. Representative seismic attribute maps utilized in this work. (A) RMS attribute map covering the hangingwall of the Lanliao Fault in Unit A, together with the isobaths of the basement of the Lanliao Fault footwall. White dashed lines denote the boundary of individual fan deltaic systems in the Eastern Trough. Blue-filled areas in the basement-depth map denote basement depressions interpreted as gorges incised in the Lanliao Fault footwall. (B) RMS attribute map covering location FLJ, Western Trough, in Unit D; faults are also represented. See Figure 3 for location of the maps.

4.4 Sandstone or siltstone thickness distributions and correlation panels

Correlation panels based on well cuttings or logs are drawn for regions of the DPD with sufficiently dense well coverage, for each study interval (units A-F). Two representative strike-oriented correlation

panels from location HZJ in the Western Trough of the basin and location WL in the axial areas centred on the Central Uplift are presented in Figure 16 and Figure 17, respectively. This work is undertaken to present the inferred lateral continuity and well connectivity of sandstone bodies.

The spatial distributions of values of sandstone or siltstone fraction are mapped for each study interval (Lower Es_3, Middle Es_3 and Upper Es_3) (Fig. 18), and isopach maps of sandstone or siltstone deposits are created for units A-F (Fig. 19). These maps are used to assist the regional palaeogeographic reconstructions, as discussed below.

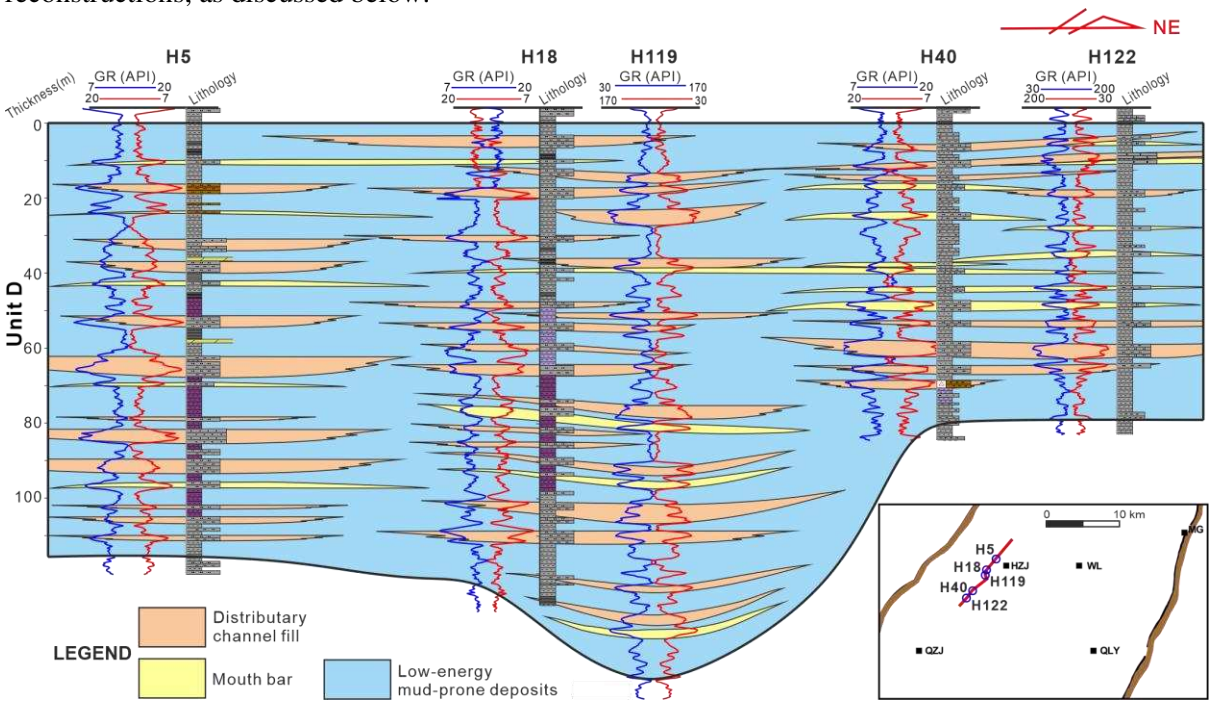

Fig. 16. Strike-oriented correlation panel for Unit D in location HZJ in the Western Trough of the basin. Correlations are based upon wireline-log response and well cuttings. GR = gamma ray. The correlation panel is hung to the top surface, which represents a flooding surface. Variation in thickness of Unit D is mainly due to the effect of intra-basin uplift. Note that the lateral extents of the sandbodies cannot be inferred reliably from the available data.

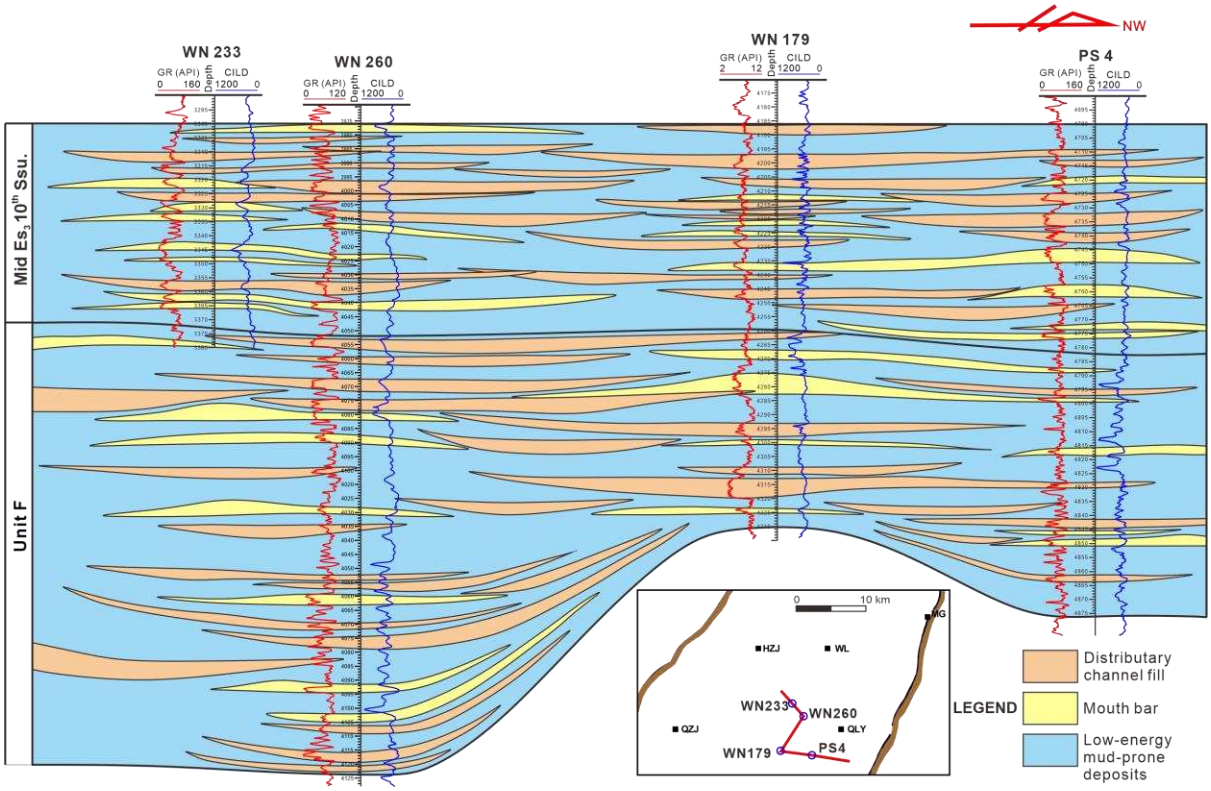

Fig. 17. Strike-oriented correlation panel for Unit F in location WL along the axial areas centred on the Central Uplift. Correlations are based upon wireline-log response. GR = gamma ray; CILD = conductivity, induction log deep; Mid = Middle; Ssu. = sandstone unit. See Figure 2 for the abbreviations of the stratigraphic units. The correlation panel is hung to the top surface, which represents a flooding surface. Variation in thickness of the intervals shown here is mainly due to the effect of intra-basin uplift. Note that the lateral extents of the sandbodies cannot be inferred reliably from the available data.

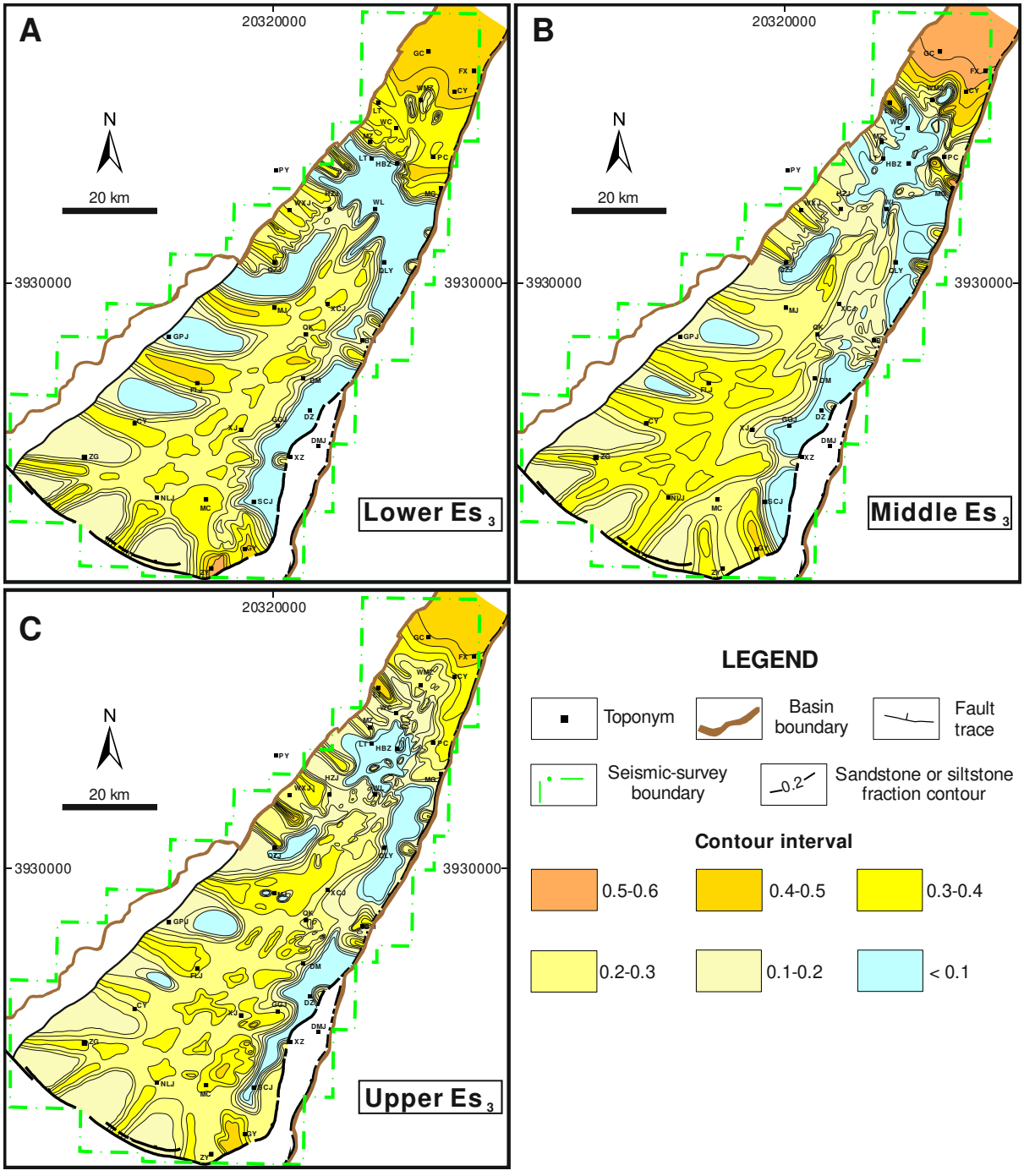

Fig. 18. Sandstone or siltstone fraction (i.e., the ratio between the cumulative thickness of sandstone or siltstone and the thickness of the overall interval) contour maps of stratigraphic units (Lower Es_3, Middle Es_3 and Upper Es_3), illustrating the position of the sandstone fairways associated with different sediment-delivery routes. Data taken from well cuttings or wireline logs of 810 wells in total. The contour interval of the maps is 0.05. Due to the sparse borehole coverage in the southwestern region, mapping of this area is only represented schematically.

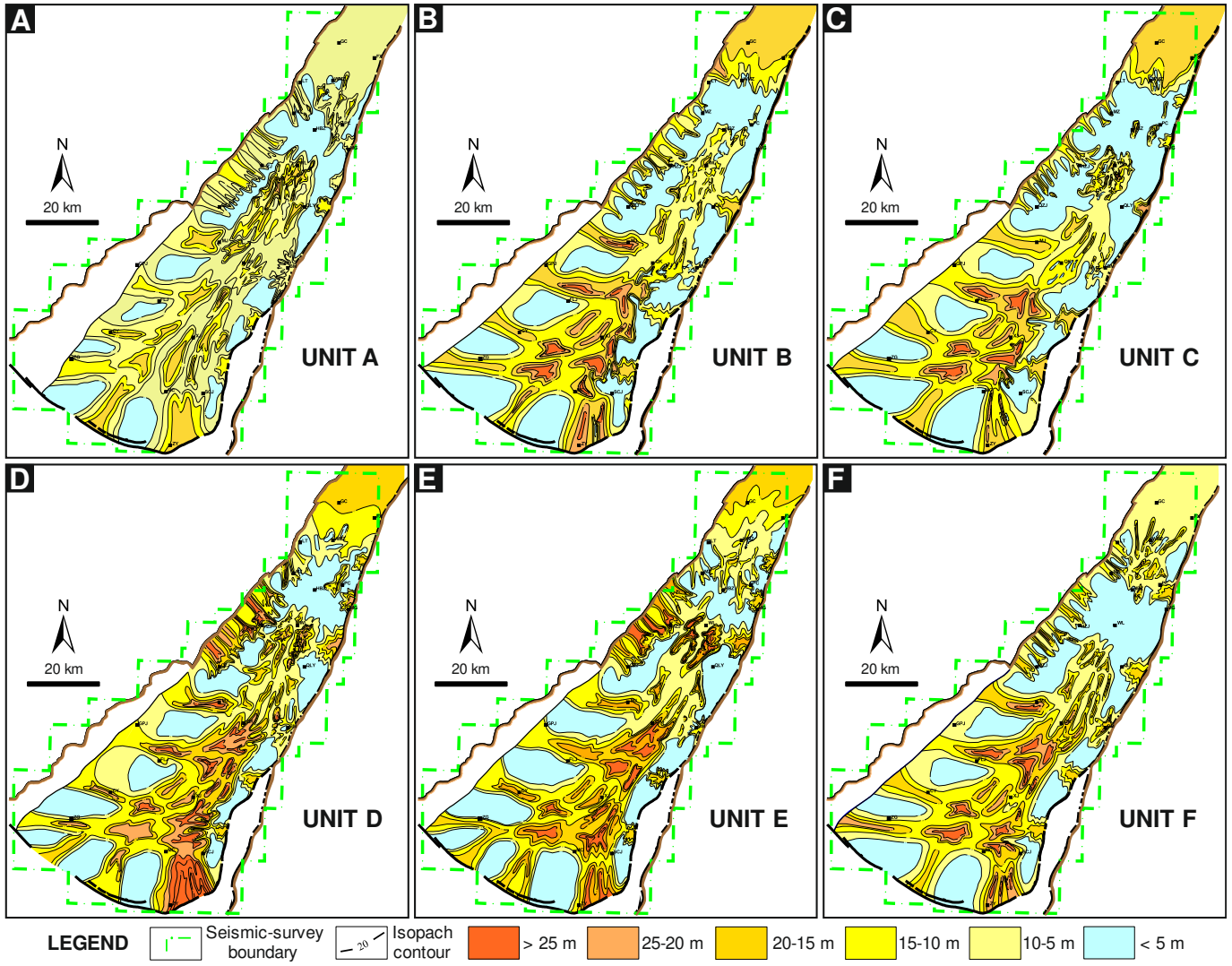

Fig. 19. Sandstone or siltstone isopach maps of units A-F, illustrating the position of the sandstone fairways associated with different sediment-delivery routes. Data taken from well cuttings or wireline logs of 947 wells. Thickness is shown as contours with units in metres. Due to the sparse borehole coverage in the southwestern region, mapping of this area is only represented schematically.

5. Discussion

5.1 Characteristics of the deltaic depositional systems

Based on the original datasets (core, wireline-log and seismic data) considered in this work and existing information from previous palaeographic studies of the DPD (Ji et al., 2005b, 2016; Yu et al., 2012), three distinct types of deltaic systems are identified in the studied stratigraphy: footwall-derived coarse-grained fan deltas, footwall-derived sand-rich deltas, and axial finer-grained deltas.

Footwall-derived fan deltas, bordering the Lanliao basin-bounding fault at the eastern edge of the basin, are typically point-sourced from the nearby footwall, and associated with small catchments (likely drainage length <10 km; see section 5.2), forming a narrow fringe adjacent to the boundary fault. In total, five footwall-derived fan deltaic systems located at MG, QLY, BM, DZ and XZ can be recognized in the DPD. The downdip length of the delta tops vary from 3.5 km to 9 km, and exhibit radially oriented elongated, likely channelized, sandbodies (Fig. 15A). Fan-delta deposits mainly comprise poorly sorted conglomerates with angular to subangular clasts, gravelly sandstones, fine to coarse sandstones and interbedded sandstones and mudstones (Fig. 5). The sandstones in these successions are dominated by feldspathic litharenite or litharenite (Fig. 5E), and by lithic arkose at location BM (Fig. 12E). In the available cores, only stream-dominated topset deposits, including alluvial channel fill and delta plain facies associations, can be reliably interpreted.

Footwall-derived sand-rich deltas, bordering the Shijaji basin-bounding fault at the northwest edge of the basin, are mainly recognized at locations HZJ and QZJ. These deltas commonly coalesced, making it difficult to differentiate individual deltaic edifices in plan view. The delta tops had radii of ca. 8 km. The foresets tend to be arranged in a progradational stacking pattern, and clinoforms dip at moderate angles (ca. 5°-10°). The deposits are typically comprised of fine to coarse-grained sandstones, which are overall finer than those forming the footwall-derived fan deltas and coarser than those forming the axial deltas, and are dominated by feldspathic litharenite, litharenite and lithic arkose (Fig. 12C). In core, distributary-channel and interdistributary-bay or -swamp facies associations could be recognized. Rare mouth-bar deposits are also interpreted.

The axial finer-grained deltaic systems represent the most widespread type of depositional system in the study area and were mainly established along the axial areas centred on the Central Uplift in the south and north of the study area. They were sourced from relatively large hinterland catchments (likely drainage length >100 km; see section 5.2). Four individual deltas in the southwest of the basin prograded into the basin in an ESE direction and their drainage networks eventually merged with those of the axial systems derived from the south and southeast, to feed the axial systems recorded at locations WL and QK. No apparent clinoform geometries are recognized. The deposits typically comprise siltstone to fine-grained sandstone with well-sorted and well to moderately rounded grains and are characterized by predominantly subarkose to lithic arkose composition (Fig. 12B). Compared to the transverse deltas, a broader range of facies associations are recognized for this type of systems in core, including distributary channel, interdistributary-bay or swamp, mouth bar, delta-front, wave-dominated or -influenced, and prodelta deposits (Figs. 7 and 8). Compared to the footwall-derived fan deltas and sand-rich deltas, mouth-bar deposits are more abundant. Notwithstanding, in this type of deltaic system, the shorelines may have been irregular or rugose in planform, at least locally, given the establishment of wave-dominated or -influenced shorelines recorded in their deposits (Bhattacharya and Giosan, 2003; Smith et al., 2005). The presence of wave-dominated or -influenced nearshore deposits is significant, given the presumably limited fetch of this lacustrine basin (Swift and Thorne, 1991), but yet consistent with recognition of wave reworking of mouth-bar and delta-front sands into marginal lacustrine beaches, spits, and barriers – similar to their marine counterparts of low to intermediate wave-energy – in certain modern lake environments. The limited gradient of the delta plains (ca. 0°-5°, average <1°) and the shallow lake-floor physiography (inferred from the seismic reflections and palaeotopographic reconstructions presented in Supporting Information 3) make this type of deltaic system particularly sensitive to lake-level changes. In response to frequent variations in lake level (1000 times/Myr; based on the analysis of lithology, assemblages of Ostracoda and spectral analysis of high-resolution gamma-ray logs; Ji et al., 2003; Wang et al., 2020), it is likely that the shorelines of the axial deltas repeatedly migrated lakeward and landward over significantly larger distances (10s of kilometres; section 5.3) compared to those of footwall-sourced deltas. Furthermore, compared to transverse deltaic systems, the gentler and shallower lake-margin bathymetry associated with the axial deltas and their higher rates of

sediment supply might have favoured more rapid delta progradation, which itself may have resulted in a relatively higher frequency of avulsion of distributary channels (Bryant et al., 1995; Ashworth et al., 2004; Jerolmack and Mohrig, 2007; Fig. 17).

5.2 Sediment provenance and relationship between axial and transverse drainages

Understanding of source areas and sediment routing in a source-to-sink perspective can help predict the spatial and temporal distribution of reservoir-quality sediments in syn-rift basin fills, and refine regional palaeogeographic reconstructions. The provenance of the studied stratigraphic units (Es_3) across the DPD remains poorly constrained: previous provenance studies either focused primarily on a local fault block (Yu et al., 2012) or utilized a single provenance technique (e.g., Jin et al., 2019). Here, the nature of sediment sources during Es_3 times has been assessed through integration of data on sediment petrography, heavy-mineral assemblages, conglomerate-clast composition (Jin et al., 2019), sandstone or siltstone fraction, and considering existing palaeotopographic reconstructions, potential palaeoslope indicators (e.g., orientation of facies belts, seismic reflections) and analysis of the exposed rock formations in potential source areas. On this basis, the relative dominance and interaction of axial and transverse depositional systems in the preserved stratigraphic record can also be investigated.

Determination of the provenance of sedimentary rocks based on compositional data analysis can provide important information on the tectonic setting of the source areas (Dickinson, 1970; Dickinson and Suczek, 1979). QFL plots for sandstone or siltstone of the DPD (Lower Es_3, Middle Es_3 and Upper Es_3) are shown in Figure 20. Compositional data for all the stratigraphic units plot over the recycled-orogen and continental-block fields of the ternary diagram, with only few readings falling in the magmatic-arc sector. This is interpreted to suggest the mixing of at least two distinct sources for the DPD, which appear to have remained active throughout the stratigraphy (Fig. 20). When considered for different regions, compositional data for the Western Trough (locations HZJ and QZJ) mostly demonstrate affinity with a recycled-orogen source; compositional data for axial areas centred on the Central Uplift (locations SCJ, MC, QK, WL, PC, WC and GYJ) are more variable, and compatible with both recycled-orogen and continental-block sources; compositional data for the Eastern Trough (locations BM and QLY) are mostly indicative of a recycled-orogen source, albeit with very few readings compatible with a magmatic-arc provenance.

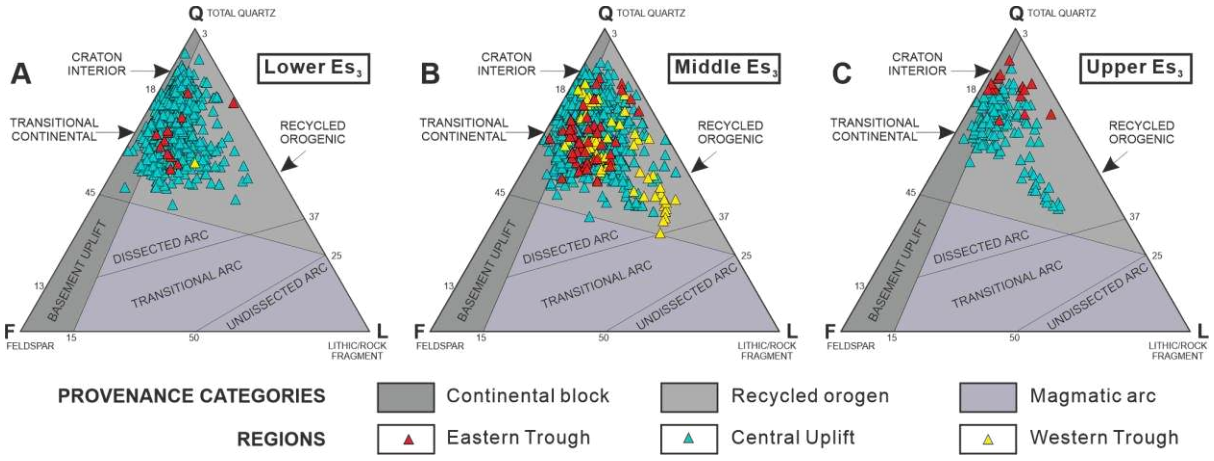

Fig. 20. Ternary diagram showing provenance data for sandstone or siltstone of the DPD for the studied intervals (Lower Es_3, Middle Es_3 and Upper Es_3), with provenance categories based on scheme by Dickinson and Suczek (1979). Data are colour-coded by different regions (Eastern Trough, Central Uplift and Western Trough). Q = Quartz; F = Feldspar; L = Lithic grains.

Based on the findings presented above, five principal possible sources are proposed for the DPD deposits of the studied stratigraphic units (Lower Es_3, Middle Es_3 and Upper Es_3), respectively feeding one transverse sediment-routing system from the east, one transverse system from the west, two axial systems from the north and south, and one transverse system from the southwest. Detailed descriptions of the potential source areas are included in Table 4. A series of transverse coarse-grained fan deltas (at locations MG, QLY, BM and DZ) lying on the Lanliao Fault hangingwall in the eastern edge of the

basin are proposed to be point-sourced by small catchments developed along the rift margin or from the major rift hinterland drainages in the Luxi Uplift. The Neihuang Uplift in the western edge of the basin is inferred to have delivered sediment to the transverse footwall-derived sand-rich deltas at locations HZJ and QZJ, near the western basin-bounding faults. The provenance of the axial finer-grained deltaic systems in the north and south is more uncertain. For the northern axial deltas, a northerly source from the Shenxian Sag or the Maling Fault zone might seem most likely. However, petrographic, heavy-mineral and conglomerate-clast-composition data indicates that these areas did not actually represent major sediment sources. Therefore, extrabasinal sources associated with relatively longer transport distance, such as the Taihang Range and the Neihuang Uplift, are inferred to have been the main contributors of terrigenous material to the northern finer-grained deltas. The widespread finer-grained deltaic systems developed along the axial areas centred on the Central Uplift in the south are interpreted to have been fed by two potential sources, i.e., by the Lankao Uplift to the south of the basin and by the Taihang Range, which was located ca. 100 km to the west of the DPD. A southerly axial system with direct sediment delivery by the Lankao Uplift seems the most parsimonious interpretation; this source area might have supplied a significant proportion of the material forming the deltaic systems observed at locations SCJ, MC and XJ. Based on observations of textural and compositional maturity, heavy-mineral assemblage, conglomerate-clast composition, and palaeogradient indicators (e.g., orientation of facies belts, seismic reflections), the axial deltaic systems seen at locations WL and QK were likely fed by an extrabasinal source area located southeast of the Taihang Range. From this area, sediment was likely delivered to the basin through a transverse drainage with an ENE direction, which then deflected towards the northeast (downstream), before merging with an axial drainage carrying sediment derived from the Lankao Uplift and eventually reaching locations QK and WL. Additionally, the observed variability in heavy-mineral characteristics at location WL, and differences in heavy-mineral assemblages and lithic-fragment types observed for samples from the east of QK relative to those from the west, suggest local interactions of the axial drainage systems with the footwall-derived transverse systems.

The degree and manner of interaction of axial and transverse depositional systems during rifting is relatively poorly documented (e.g., in the East African Rift System; Soreghan et al., 1999; Zhang and Scholz, 2015; in the Corinth Rift; Gawthorpe et al., 2018; Cullen et al., 2019; in the North Sea; McArthur et al., 2016; and in the Dampier Sub-basin of the Northwest Shelf of Australia; Chen et al., 2020). One outstanding question is what controls how axial and transverse systems interact, and whether this interaction reflects the balance between rates of transverse and axial sediment flux and local tectonics (Mack and Leeder, 1999; Gawthorpe and Leeder, 2000; Leeder and Mack, 2001). Most studies have hitherto examined the interaction between axial and transverse systems in purely alluvial settings, where, for example, it is observed that repeated toe-cutting of transverse footwall-derived alluvial fans by axial rivers can be driven by local tectonic mechanisms including fault growth and hangingwall tilting (e.g., Mack and Leeder, 1999; Leeder and Mack, 2001). This work offers some insight into the interaction of axial and transverse depositional systems in syn-rift basins with shallow-water lakes. The interaction and amalgamation of transverse systems and axial systems recognized in the stratigraphy examined at locations QK and WL is attributed to the presence of local basinal highs that initially controlled sediment-delivery pathways, and by high rates of sediment supply that enabled isolated depocentres to be overfilled and to ultimately link together.

The relative dominance of axial versus transverse depositional systems in the basin fill is also demonstrated. This serves as a quantitative analogue study for the relative preservation of axial and transverse systems in this type of asymmetric extensional basins during the syn-rift stage. Based on plan-view quantification of the palaeogeographic maps (see section 5.3), the axial depositional systems represent the most widespread sedimentary systems in the basin, covering a much larger fraction (ca. 85%) than their transverse counterparts in the DPD (ca. 15%), with the latter only distributed as a discontinuous narrow fringe along the basin-bounding faults. Based on pseudo-3D quantifications of volumes from correlation panels, the axial depositional systems cover an even larger fraction (ca. 90%) of the preserved stratigraphic record. The predominance of axial depositional systems relative to transverse systems in the basin fill is attributed to a series of factors, including the significantly larger size of their catchment areas and the resultant higher rates of sediment supply (Syvitski and Milliman, 2007).

Table 4. Potential source areas of the studied DPD stratigraphy.

Region name and drainage orientation	**Description of potential source area**	**Transport distance from headwaters**
Luxi Uplift, transverse-east	- Proximal source to Lanliao Fault hangingwall fan deltas, as inferred based on proximity to the basin edge along the footwall block (Fig. 1C). - Compatible with presence of drainage outlets deeply incised into the basement of the footwall block (Fig. 15A) and southward palaeoslopes shown in the seismic reflections. - Compatible with limited compositional and textural maturity (Fig. 12E) and inferred short transport distance. - Potentially exposed Palaeozoic carbonate and siliciclastic rocks and Mesozoic volcanics in the Luxi Uplift during the Eocene (Jin et al., 2019), compatible with composition of fan-delta deposits: lithic fragments dominated by sedimentary and metamorphic lithics (Fig. 13), heavy-mineral assemblages abundant in magnetite (Fig. 14) and conglomerate-clast composition mainly comprising of micrite, bioclastic limestone and calcareous sandstone and subordinate mudstone, basalt and quartzite (Jin et al., 2019).	Short (<10 km)
Neihuang Uplift, transverse-west	- Proximal source to the sand-rich deltas in locations HZJ and QZJ, as inferred based on proximity to the basin edge along the footwall block (Fig. 1C). - Compatible with limited compositional and textural maturity (litharenites to feldspathic litharenites with average maturity index of 1.51; Fig. 12C) and inferred short transport distance. - Potentially exposed Upper Palaeozoic siliciclastic and carbonate rocks, Precambrian metamorphic basement, and Mesozoic intrusive and siliciclastic rocks in the Neihuang Uplift during the Eocene (Jin et al., 2019), compatible with composition of sand-rich deltaic deposits: lithic fragments mainly composed of sedimentary lithics, subordinate metamorphic lithics, and low to absent volcanic lithics (Fig. 13), heavy-mineral assemblages dominated by garnet (max. 82%), perovskite (max. 50%) and magnetite (max. 30%) (Fig. 14) and conglomerate-clast composition including calcareous sandstone, quartz arenite, flint, sandy limestone, micrite and dolomite (Jin et al., 2019).	Short (<10 km)
Taihang Range+Neihuang Uplift, axial-north	- Shenxian Sag or Maling Fault zone: likely proximal sources to the axial deltas in the north, as inferred based on proximity to the basin edge (Fig. 1C). - The Taihang Range and Neihuang Uplift, unlike the Shenxian Sag or Maling Fault Zone, likely exposed Mesozoic clastics, Upper Palaeozoic carbonates and clastics, and the Precambrian metamorphic basement during the Eocene (Jin et al., 2019), based on the characteristics of the axial deltaic deposits: heavy-mineral assemblages dominated by zircon (20-72%), garnet (30%-45%) and tourmaline (10-20%) (Fig. 14), lithic fragments dominated by a mixing of sedimentary, volcanic and metamorphic rocks (Fig. 13), and conglomerate-clast composition dominated by quartz arenite, flint, micrite, volcanic rock, intermediate to acid intrusive rock, granite gneiss and quartzite (Jin et al., 2019). - The Taihang Range and Neihuang Uplift are interpreted as major sources in view of grainsize and compositional and textural maturity of the axial deltaic deposits in the north (Fig. 12A) and knowledge of the geological composition of the various blocks surrounding the DPD during the Eocene (Jin et al., 2019); sediment derivation from	Long (>100 km)

	the Shenxian Sag or Maling Fault zone cannot be ruled out, but these domains would have hosted small catchments.	
Lankao Uplift, axial-southeast	- Proximal source to axial deltas in the south (locations SCJ, MC and XJ), as inferred based on proximity to the basin edge (Fig. 1C). - Compatible with relatively limited compositional and textural maturity (Fig. 12F) and inferred relatively limited short transport distance. - Potentially exposed Upper Palaeozoic carbonates and clastics, Mesozoic extrusives, and the Precambrian metamorphic basement in the Lankao Uplift during the Eocene (Jin et al., 2019), compatible with composition of axial deltaic deposits in the south: mixed lithic fragments, heavy-mineral assemblages dominated by garnet and zircon and conglomerate-clast composition dominated by micrite, bioclastic limestone, volcanic tuff, calcareous sandstone and low to absent quartzite (Jin et al., 2019). - Also compatible with spatial variations in proportions of volcanic lithics and maturity index (1.69 to 2.01), indicating the transport distance as increasing northward away from the Lankao Uplift (Slatt and Eyles, 1981; Phillips, 2007; McKellar et al., 2020).	Relatively short (10s km)
Southeast of Taihang Range, transverse to axial-southwest	- Main source to the transverse deltas in the southwest areas of the basin and to the axial finer-grained deltas at locations QK and WL (Fig. 1C). - Compatible with higher compositional (subarkose to arkose; average maturity index of 2.46; Fig. 12B) and textural maturity (well sorted, subrounded to rounded grains) and inferred longer transport distance for the axial deltaic deposits. - Compatible with sediment supplied to the depocentre through the observed ENE drainage vector. - Compatible with direction of progradation seen in seismic reflections, sandstone/siltstone fraction distribution, heavy mineral characteristics and compositional maturity trends: 1) ENE clinoform progradation in the southwest (locations FLJ, GPJ, SCJ and MGJ); 2) marked reduction in the proportion of unstable volcanic lithics and maturity from locations FLJ and MJ to location QK (samples from PS8 contain ca. 30% volcanic lithics and have maturity index of 1.50; samples from QK are mostly lithic arkose and subordinate subarkose, are dominated by sedimentary and metamorphic lithics, and have average maturity index of 2.46). - Potentially exposed Mesozoic siliciclastic rocks, Precambrian crystalline metamorphic rocks, and Upper Palaeozoic carbonates and clastics in the Taihang Range during the Eocene (Jin et al., 2019) are compatible with composition of transverse and axial deltaic deposits (Jin et al., 2019).	Long (>100 km)

5.3 Palaeogeographic reconstructions for DPD Es_3 stratigraphic units

Stratigraphic and spatial variations in syn-rift sedimentary architectures result from the interplay of tectonic, base-level, and climatic controls, which affect basin and catchment-area characteristics (Gawthorpe and Leeder, 2000; Gawthorpe et al., 2018). A summary of the palaeogeography of the DPD for the syn-rift Es_3 stratigraphic units is presented (Fig. 21). During Lower Es_3 times (Fig. 21F), the activity of the boundary faults and of the NNE-SSW-striking Huanghe-Wenxi-Guancheng Fault system likely enhanced the development of the transverse footwall-derived coarse-grained fan deltas on the hangingwall of the Lanliao Fault, to the east, and of the transverse footwall-derived sand-rich deltas on the hangingwalls of the western boundary faults (Wuxingji, Shijiaji and Changyuan Faults). Simultaneously, axial finer-grained deltaic systems developed along the areas centred on the Central Uplift in the south and north of the study area. During the deposition of unit F (Fig. 21F), five footwall-derived fan deltas (located at MG, QLY, BM, DZ and XZ) grew on the Lanliao Fault hangingwall, whose delta tops were typically <7 km in planform diameter. Of these, the fan delta located at BM was comparatively larger in scale, and is characterized by deposits that are relatively cleaner, better sorted

and more mature. This might be due to the presence of a relay ramp at this location along the rift margin as imaged in seismic data by Liang et al. (2011), which may have connected this deltaic system to hinterland catchments that were relatively larger than those of other deltaic systems along the basin margin (Gupta et al., 1999; Young et al., 2000; Athmer and Luthi, 2011), and associated with relatively higher rates of sediment supply and longer transport distance (Athmer and Luthi, 2011; McArthur et al., 2016). Among the footwall-derived sand-rich deltas occurring on the northwestern margin of the basin, two distinct deltaic complexes can be recognized: one at location MZ and the other one covering locations HZJ and QZJ. The drainage networks of both deltas generally flowed towards southeast, with drainage of one delta merging with that of an axial system distally. The orientation of these drainage networks was again primarily controlled by the orientation of the relay-ramp zones of these faults as imaged in seismic data (Ye et al., 2008): these sand-rich deltas potentially enter the basin via these relay zones. In the north of the basin, widespread axial finer-grained deltas developed, with depositional systems with northerly, northwesterly and northeasterly provenance coalescing at location GYJ and then prograding to the SW to reach the areas of P99-W83-W311-P16. The southwest and southeast of the study area were dominated by large axial finer-grained deltas. Three transverse deltaic systems at locations MJ, FLJ and CY were associated with drainage direction to ESE at their apices, which rotated to NE further downdip; the drainage networks of these systems merged with those of the southerly axial depositional systems derived from the Lankao Uplift, to eventually deliver sediment at locations QK and WL. Evaporitic saline-lake deposits developed around location WL in the northern-central part of the basin, over an area of ca. 100 km^2. Nine depocentres in the study area can be identified during this period, each of which accumulated a thick succession of lacustrine mudstone.

During the Middle Es_3 period (Fig. 21B-E), fault activity in the basin intensified (Yu et al., 2019; Zhu et al., 2020), resulting in increased subsidence rates – and rates of creation of accommodation – relative to sediment-supply rates, especially near to the basin margins. This period was therefore characterized by widespread lake transgression, overall retrogradation of the deltaic systems, and reduction of the size of the lake sector undergoing deposition of evaporites: as the climate became more humid and warmer, the salinity of the lake decreased (Yu et al., 2012). During the times encompassing the deposition of units E to C (Fig. 21E-C), the steady lake transgression culminated in unit C, within which lacustrine mudstones are distributed over the largest area. Sporadic gravity-flow-dominated deposits accumulated over the hanging wall of the Duzhai Fault, remobilizing material from the fan deltas at location BM, and over the hangingwall of the Changyuan Fault, sourced from the sand-rich deltas at locations HZJ and QZJ. The gravitational instability of these deltas might have been driven in part by increased seismicity associated with the more intense fault activity of Middle Es_3 times.

During Upper Es_3 times (Fig. 21A), the activity of most faults in the basin waned (Yu et al., 2019; Zhu et al., 2020). Specifically, the northern part of the Lanliao Fault along the eastern margin of the basin experienced increased tectonic activity, the activity of the western basin-bounding faults waned, the activity of the Duzhai Fault ceased, whereas the activity of Huanghe-Wenxi-Guancheng Fault systems in the basin waxed. This period was characterized by lake-level regression, overall progradation of the deltaic systems, and expansion of the evaporite-dominated lake centre. Deposition by sediment gravity flows on the lake bottom, associated with the Duzhai and Changyuan faults, was subdued during this period (Fig. 21A).

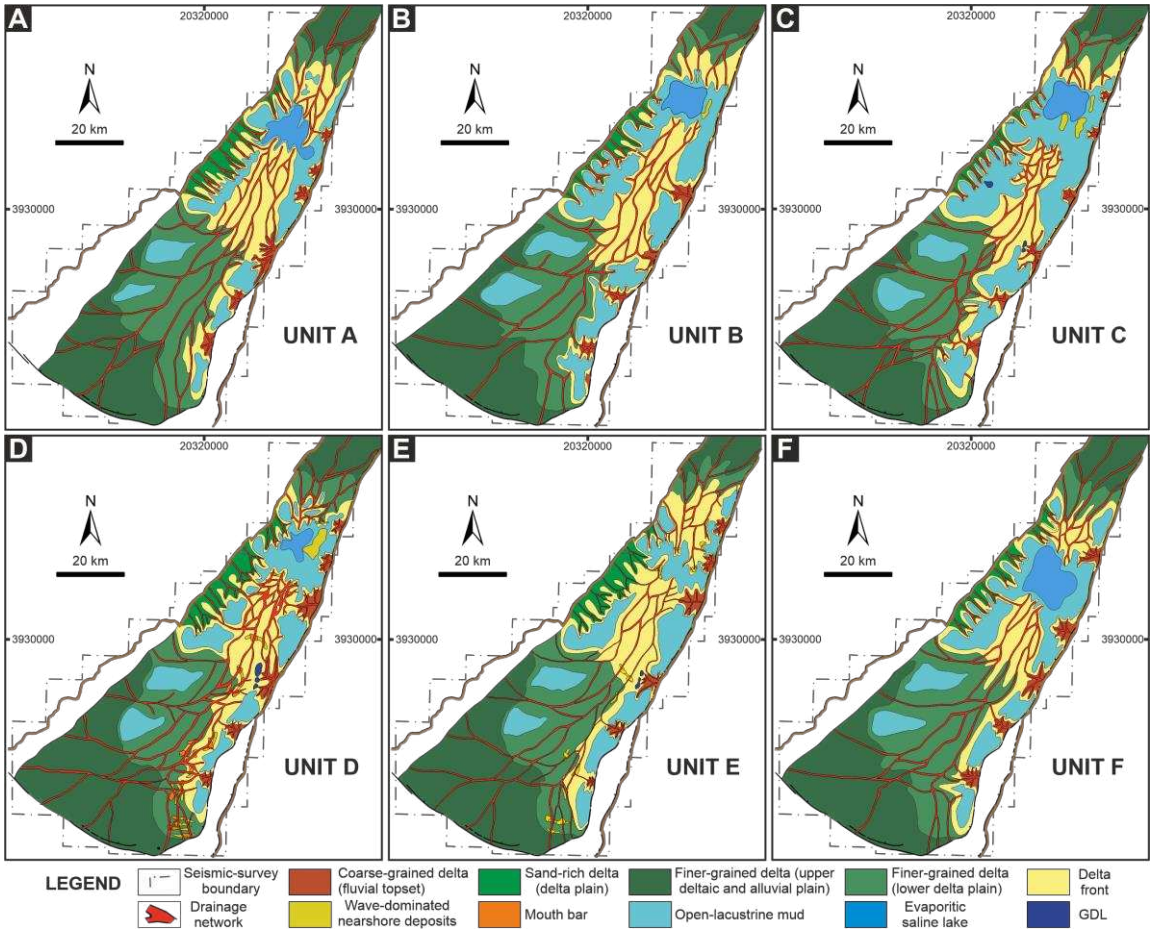

Fig. 21. Maps of interpreted gross depositional environments for the time intervals corresponding to units A-F. GDL = Gravity-flow-dominated lake-bottom deposits. Due to the sparse borehole coverage in the southwestern region, mapping of this area is only represented schematically, and the true drainage pattern of westernmost transverse streams is unknown. Note that these maps only represent the distribution of facies associations that dominate each stratigraphic interval and the dominant inferred drainage directions; none of the planforms illustrated in the maps may represent an exact paleogeographic configuration at any one point in time.

5.4 Implications for syn-rift reservoir distribution

The stratigraphic records of axial and transverse syn-rift depositional systems might differ markedly with regard to hydrocarbon-reservoir quality and distribution (Schwarz and Wood, 2016; McArthur et al., 2016; Sihombing et al., 2019). Transverse systems are usually footwall-derived alluvial fans or fan deltas sourced from limited catchments developed along the rift-margin faults, or gravity-flow-dominated deposits developed over the hangingwall of fault-controlled intra-rift footwall highs (Schwarz and Wood, 2016; Gawthorpe et al., 2018). They often have limited spatial extent and may comprise of relatively poorly sorted sediments with comparatively poor reservoir potential (Schwarz and Wood, 2016; McArthur et al., 2016), even though in some cases they can act as productive reservoir units (e.g., Somerville et al., 2020). Axial syn-rift fluvio-deltaic systems tend to be sourced from relatively larger catchments with longer transport distances, and thus tend to generate larger accumulations, generally characterized by cleaner, finer-grained, better-sorted, and more mature sediments, hence having relatively greater reservoir potential (Schwarz and Wood, 2016; McArthur et al., 2016; Sihombing et al., 2019).

In agreement with this view, in the studied stratigraphy, the axial deltaic systems were sourced from relatively large catchments and form relatively good reservoir targets (porosity φ = 15% ~ 20% and permeability K = 10×10^{-3} ~1000×10^{-3} μm^2; Song, 2016), in the form of fairly thick successions of relatively clean, well-sorted very fine to fine sandstones of distributary-channel and mouth-bar origin, which may amalgamate into packages that are up to 10 m thick (Figs. 16 and 17). In addition, these

sand-prone units commonly alternate with low-energy mud-prone overbank/interdistributary-bay/prodelta deposits, characterized by high preservation of organic matter and with potential as source rocks (north of the basin: sapropelic and humic kerogen and average TOC of 1.54%; south of the basin: partial humic and mixed kerogen and average TOC of 0.34%; Chen et al., 2012; Tang et al., 2017; Tang et al., 2020). Deltaic deposits encased in thick lacustrine mudstones represent a good reservoir target (porosity φ = 15% ~ 20% and permeability K = 10×10^{-3} ~1000×10^{-3} μm^2; Song, 2016). Particularly, the wave-dominated nearshore deposits, present as fairly thick packages (up to 10 m thick) of very-fine sandstone with well-sorted, well-rounded grains formed as a product of wave reworking and encased in thick lacustrine mudstones, represent a good reservoir target (φ = 20%~30% and K = 100×10^{-3} ~1000×10^{-3} μm^2; Song, 2016). Due to the alternation of phases of delta progradation and retrogradation in response to relative lake-level changes, nearshore deposits are also often encased in thick salt deposits (up to 600 m in Es_3), which can act as reservoir seal.

The deposits of the studied transverse fan deltas tend to have poor reservoir potential (φ < 5%, K < 0.1 $\times10^{-3}$ μm^2; Song, 2016), due to the poorly sorted nature of conglomerates with subangular to angular clasts, and to the widespread occurrence of mudstones. Furthermore, their limited size makes them small targets whose distribution is difficult to predict in the subsurface (cf. McArthur et al., 2016; Schwarz and Wood, 2016; Chen et al., 2020). However, hangingwall fans could represent viable reservoir targets where these were fed by major rift hinterland drainages, associated with comparatively high rates of sediment supply and long sediment transport distances. This might be the case for the reservoir-quality sandstones deposited at location BM (φ = 10%~15% and K = 10×10^{-3} ~100×10^{-3} μm^2; Song, 2016), associated with a deltaic system that was considerably larger than the other footwall-derived fan deltas (Fig. 21). Prediction of oversized hangingwall fans in the subsurface is challenging, but possible predictive approaches include: 1) mapping the depth contours for the basement of the bounding fault footwall, so as to attempt the identification of basin-margin drainage outlets, the scale of which may correlate with the corresponding drainage area and hence with the resultant hangingwall fan; and 2) attempting to locate the position of relay ramps in seismic data, as relay ramps may connect to larger catchments characterized by higher rates of sediment supply and longer transport distance.

6. Conclusions

In this study, an integration of seismic, wireline-log, core, petrographic, and heavy-mineral datasets and existing palaeotopographic reconstructions has been utilized to characterize the sedimentology and stratigraphic architecture of syn-rift depositional systems of a lacustrine basin and to determine the spatiotemporal distribution and reservoir potential of axial and transverse sediment-routing systems. The main findings are summarized as follows.

- Three distinct types of deltaic systems are identified in the studied succession: footwall-derived coarse-grained fan deltas, footwall-derived sand-rich deltas, and axial finer-grained deltas. The spatiotemporal distribution of the deposits of these systems in this syn-rift basin fill is attributed to the interplay of tectonic, lake-level and climatic controls.
- The nature of sediment sources of the DPD deposits has been assessed during Es_3 times: the transverse coarse-grained fan deltas are inferred to have been fed by small point-source catchments developed along the basin margin or from the major rift hinterland drainages in the Luxi Uplift; the transverse footwall-derived sand-rich deltas near the western basin-bounding faults are inferred to have been sourced from the Neihuang Uplift in the western edge of the basin; the axial deltaic systems in the north were possibly sourced, mainly, from the Taihang Range and the Neihuang Uplift, with a subordinate component from the Shenxian Sag or the Maling Fault zone; the axial deltas centred on the Central Uplift in the south were likely fed by two potential sources: the Lankao Uplift to the south of the basin and the Taihang Range located ca. 100 km to the west of the DPD.
- The interaction and amalgamation of transverse systems and axial systems recognized locally in the stratigraphy are attributed to the presence of local basinal highs that controlled sediment-delivery pathways, and by high sediment-supply rates that caused overfilling and linkage of isolated depocentres.
- Reconstruction of the relative dominance of axial versus transverse depositional systems in the basin fill demonstrates that axial systems predominate (>85% of stratigraphy) over transverse systems.
- The axial deltaic systems represent spatially extensive depositional units containing relatively good reservoir targets, sourced from relatively large catchments and comprising of relatively clean, well-

sorted very-fine to fine sandstone. The deposits of the studied transverse fan deltas tend to have poorer reservoir potential, due to the poor sorting and clast angularity of conglomeratic deposits, despite potentially representing viable reservoir targets locally. Prediction of the position of oversized deltas can be attempted by locating relay ramps in seismic data, and by identifying basin margin drainage outlets carved in the basement of footwall blocks.

Acknowledgements

This research was financially supported by the National Natural Science Foundation of China (No. 41672098) and Zhongyuan Oilfield, Sinopec, China. The Research Institute of Exploration and Development, Zhongyuan Oilfield, Sinopec, is thanked for their support in providing original data utilized in this research and for the permission to publish the results. LC and NPM thank the sponsors and partners of FRG-ERG and SMRG for financial support: AkerBP, Areva (now Orano), BHPBilliton, Cairn India (Vedanta), ConocoPhillips, Chevron, Debmarine, Engie, Equinor, Murphy Oil, Nexen-CNOOC, Occidental, Petrotechnical Data Systems, Saudi Aramco, Shell, Tullow Oil, Woodside and YPF. Dave Somerville and Dave Hodgson are thanked for providing constructive discussion on various aspects of this work. We thank Associate Editor Roberto Tinterri, Prof. Finn Surlyk and two anonymous reviewers for their constructive comments, which considerably improved the paper.

References

Allen, J.R.L., 1963. Asymmetrical ripple marks and the origin of water-laid cosets of cross-strata. Geol. J. 3, 187-236.

Allen, J.R.L., 1968. Current Ripples: Their Relation to Patterns of Water and Sediment Motion. North-Holland Publishing Company, Amsterdam, 433 pp.

Allen, J. R. L. 1979. A model for the interpretation of wave ripple-marks using their wavelength, textural composition, and shape. J. Geol. Soc. Lond. 136, 673-82.

Allen, P. A. 1981. Some guidelines in reconstructing ancient sea conditions from wave ripple marks. Marine Oeol. 43, M59-67.

Allen, J.R.L., 1982. Sedimentary Structures, their Character and Physical Basis, Volumes 1, 2. Elsevier, Amsterdam.

Allen, J.R.L., 1985, Principles of Physical Sedimentology. Allen and Unwin, London, pp. 196.

Arnott, R.W.C., Hand, B.M., 1989. Bedforms, primary structures and grain fabric in the presence of suspended sediment rain. J. Sed. Res. 59, 1062–1069.

Ashworth, P.J., Best, J.L., Jones, M., 2004. Relationship between sediment supply and avulsion frequency in braided rivers. Geology 32, 21–24.

Athmer, W., Luthi, S.M., 2011. The effect of relay ramps on sediment routes and deposition: A review. Sediment. Geol. 242, 1–17.

Athy, L.F., 1930. Density, porosity and compaction of sedimentary rocks. Am. Assoc. Pet. Geol. Bull. 14, 1-24.

Best, J.L., Bridge, J.S., 1992. The morphology and dynamics of low amplitude bedwaves upon upper stage plane beds and the preservation of planar laminae. Sedimentology 39, 737–752.

Bhattacharya, J., Walker, R.G., 1991. River-dominated and wave-dominated depositional systems of the Upper Cretaceous Dunvegan Formation, Northwestern Alberta. Bull. Can. Petroleum Geol. 39, 165-191.

Bhattacharya, J.P., 2006. Deltas. In: Posamentier H.W., Walker R.G. (Eds.), Facies Models Revisited. SEPM Spec. Publ. 84, 237–292.

Bhattacharya, J.P., Giosan, L., 2003. Wave-influenced deltas: geomorphological implications for facies reconstruction. Sedimentology 50, 187–201.

Bouma, A.H., 1962. Sedimentology of Some Flysch Deposits: a Graphic Approach to Facies Interpretation. Elsevier Publishing Company, Amsterdam, pp. 168.

Bray Jr, T.F., Carter, C.H., 1992. Physical processes and sedimentary record of a modern, transgressive, lacustrine barrier island. Mar. Geol. 105, 155–168.

Bridge, J.S., Best, J.L., 1988. Flow, sediment transport and bedform dynamics over the transition from dunes to upper-stage plane beds: implications for the formation of planar laminae. Sedimentology 35, 753–763.

Bridge, J.S., Demicco, R.V., 2008. Earth Surface Processes, Landforms and Sediment Deposits. Oxford University Press, Cambridge, 815 pp.

Bryant, M., Falk, P., Paola, C., 1995. Experimental study of avulsion frequency and rate of deposition. Geology 23, 365-368.

Chen, H., Wood, L.J., Gawthorpe, R.L., 2020. Sediment dispersal and redistributive processes in axial and transverse deep-time source-to-sink systems of marine rift basins: Dampier Sub-basin, Northwest Shelf, Australia. Basin Res. 1–23.

Chen, J., Lu, K., Feng, Y., Yuan, K., Wang, D., Cui, H., 2012. Evaluation on hydrocarbon source rocks in different environments and characteristics of hydrocarbon generation and expulsion in Dongpu Depression. Fault-Block Oil Gas Field 19, 35–38.

Chen, S.P., Qi, J.F., Wang, D.R., Cheng, X.S., Zhao, Y.B., Xu, Z.Q., Xie, C., Sun, H.L., 2007. Fault systems and transfer structures in Dongpu Sag. Arcta Petrolei Sinica 28 (in Chinese with English Abstract).

Cullen, T.M., Collier, R.E.L., Gawthorpe, R.L., Hodgson, D.M., Barrett, B.J., 2019. Axial and transverse deep-water sediment supply to syn-rift fault terraces: Insights from the West Xylokastro Fault Block, Gulf of Corinth, Greece. Basin Res. 1–35.

Davies, I.C., Walker, R.G., 1974. Transport and deposition of resedimented conglomerates; the Cap Enrage Formation, Cambro-Ordovician, Gaspe, Quebec. J. Sediment. Res. 44, 1200-1216.

Demaison, G.J., Moore, G.T., 1980. Anoxic environments and oil source bed genesis. AAPG Bull. 64, 1179–1209.

Dickinson, W., 1970. Interpreting detrital modes of graywacke and arkose. J. Sediment. Res. 40, 695–707.

Dickinson, W.R., Suczek, C.A. 1979. Plate tectonics and sandstone compositions. Am. Assoc. Pet. Geol. Bull.63, 2164–2182.

Dott Jr, R.H., Bourgeois, J., 1982. Hummocky stratification: significance of its variable bedding sequences. Geol. Soc. Am. Bull. 93, 663-680.

Fielding, C.R., 2006. Upper flow regime sheets, lenses and scour fills: extending the range of architectural elements for fluvial sediment bodies. Sediment. Geol. 190, 227-240.

Fisher, R.V., 1971. Features of coarse-grained, high-concentration fluids and their deposits. J. Sediment. Res. 41, 916-927.

Folk, R.L., 1980. Petrology of sedimentary rocks. Hamphills, Austin Texas. 170 p.

Garland, C., Haughton, P., King, R., Moulds, T., 1999. Capturing reservoir heterogeneity in a sand-rich submarine fan, Miller Field. In: Fleet, A., Boldy, S.A. (Eds.), Petroleum geology of north- west Europe. Proceedings of the 5th conference, London, UK, Geological Society of London, pp. 1199–1208.

Gawthorpe, R.L., Leeder, M.R., 2000. Tectono-sedimentary evolution of active extensional basins. Basin Res. 12, 195–218.

Gawthorpe, R.L., Leeder, M.R., Kranis, H., Skourtsos, E., Andrews, J.E., Henstra, G.A., Mack, G.H., Muravchik, M., Turner, J.A., Stamatakis, M., 2018. Tectono-sedimentary evolution of the Plio-Pleistocene Corinth rift, Greece. Basin Res. 30, 448–479.

Gupta, S., Underhill, J.R., Sharp, I.R., Gawthorpe, R.L., 1999. Role of fault interactions in controlling synrift sediment dispersal patterns: Miocene, Abu Alaqa Group, Suez rift, Sinai, Egypt. Basin Res. 11, 167–189.

Halfman, J.D., 1993. Water column characteristics from modern CTD data, Lake Malawi, Africa. J. Great Lakes Res. 19, 512-520.

Henry, P.H., 1996. Analysis of sonic well logs applied to erosion estimates in the Bighorn basin, Wyomin. Am. Assoc. Pet. Geol. Bull. 80, 630-647.

Hou, G.T., Qian, X.L., Cai, D.S., 2001. The tectonic evolution of Bohai basin in Mesozoic and Cenozoic time. Acta Sci. Nat. Univ. Pekin. 37, 845-851 (in Chinese).

Hubert, J.F., 1962. A zircon-tourmaline-rutile maturity index and the interdependence of the composition of heavy mineral assemblages with the gross composition and texture of sandstones. J. Sediment. Res. 32, 440-450.

Jelby, M.E., Grundvåg, S.A., Helland-Hansen, W., Olaussen, S., Stemmerik, L., 2020. Tempestite facies variability and storm-depositional processes across a wide ramp: Towards a polygenetic model for hummocky cross-stratification. Sedimentology 67, 742-781.

Jerolmack, D.J., Mohrig, D., 2007. Conditions for branching in depositional rivers. Geology 35, 463-466.

Ji, Y.L., Fang, J., Wang, S., Tan, Y., Zhang, H., Wang, D., 2003. High frequency lake-level change of 3rd Member of Shahejie Formation and prediction of lowstand sandbody in Dongpu Depression. Geological Journal of China Universities 9 (in Chinese with English Abstract).

Ji, Y.L., Fang, J., Wang, S., Tan, Y., Zhang, H., Wang, D., 2005a. Origin of salt and gypsum rock in the third member of Shahejie formation of lower tertiary in Dongpu depression. Acta Sedimentol. Sin. 23, 225–231 (in Chinese with English Abstract).

Ji, Y.L., Feng, J.H., Wang, S.L., Zhang, H.A., Wang, D.R., 2005b. Shifting of lake shoreline and lithofacies palaeogeographic characters during sedimentary period of the Member 3 of Shahejie Formation of Paleogene in Dongpu Sag. Journal of Pelaeogeography 7, 1505-1671 (in Chinese with English Abstract).

Ji, Y.L., Wang, R., Song, H.Y., Li, D.J., Zhou S., Li, L.D., 2016. Palaeogeographic reconstruction and reservoir evaluation of Palaeogene, Dongpu Depocentre, Bohai Bay Basin, China. Unpublished internal report, China University of Petroleum (Beijing).

Jiang, Y.L., Chang, Z. H., Lu, X. S., Wu, X. L., 2008. Genetic types and distribution of paleogene condensate gas pools in Dongpu Depression. Journal of China University of Petroleum (Edition of Natural Science) 32, 28–34 (in Chinese with English Abstract).

Jin, Y.Q., Yang, D.D., Jiang, F.H., Jin, K.K., 2019. The sedimentary filling characteristics of clastic rocks and their responses to tectonic activities in Dongpu depression. Science Technology and Engineering 19, 83-89 (in Chinese with English Abstract).

Johnson, M.J., 1993. The system controlling the composition of clastic sediments. Geol. Soc. Am. Spec. Pap. 284, 1–20.

Jones, M. A., Cronin, B. T., Allerton, S., 2018. A depositional model for the T-block Thelma field, UKCS block 16/17. In: Turner, C.C., Cronin, B.T. (Eds.), Rift-related coarse-grained submarine fan reservoirs; The Brae Play, South Viking Graben, North Sea. AAPG Mem. 115, 307–338. Tulsa, Oklahoma, American Association of Petroleum Geologists.

Keighley, D., 2008. A lacustrine shoreface succession in the Albert Formation, Moncton Basin, New Brunswick. Bull. Can. Petrol Geol. 56, 235–258.

Kiro, Y., Goldstein, S.L., Garcia-Veigas, J., Levy, E., Kushnir, Y., Stein, M., Lazar, B., 2017. Relationships between lake-level changes and water and salt budgets in the Dead Sea during extreme aridities in the Eastern Mediterranean. Earth Planet. Sci. Lett. 464, 211–226.

Kneller, B., 1995. Beyond the turbidite paradigm: physical models for deposition of turbidites and their implications for reservoir prediction. In: Hartley, A.J., Prosser, D.J. (Eds.), Characterisation of Deep Marine Clastic Systems. Geol. Soc. London Spec. Publ. 94, 29–46.

Kneller, B.C., Branney, M.J., 1995. Sustained high- density turbidity currents and the deposition of thick massive sands. Sedimentology 42, 607–616.

Kumar, N., 1979. Thickness of removed sedimentary rocks, paleopore pressure, and paleotemperature, southwestern part of Western Canada basin: discussion. Am. Assoc. Pet. Geol. Bull. 63, 812-814.

Leckie, D.A., Walker, R.G., 1982. Storm-and tide-dominated shorelines in Cretaceous Moosebar-Lower Gates interval—outcrop equivalents of Deep Basin gas trap in western Canada. Am Assoc Pet Geol Bull. 66, 138-157.

Leeder, M.R., Mack, G.H., 2001. Lateral erosion ('toe-cutting') of alluvial fans by axial rivers: Implications for basin analysis and architecture. J. Geol. Soc. London. 158, 885–894.

Leeder, M.R., Mack, G.H., Salyards, S.L., 1996. Axial-transverse fluvial interactions in half-graben: Plio-Pleistocene Palomas Basin, southern Río Grande Rift, New Mexico, USA. Basin Res. 12, 225–241.

Leppard, C.W., Gawthorpe, R.L., 2006. Sedimentology of rift climax deep water systems; lower rudeis formation, hammam faraun fault block, Suez Rift, Egypt. Sediment. Geol. 191, 67-87.

Li, S., Zhao, G., Dai, L., Zhou, L., Liu, X., Suo, Y., Santosh, M., 2012. Cenozoic faulting of the Bohai Bay Basin and its bearing on the destruction of the eastern North China Craton. J. Asian Earth Sci. 47, 80–93.

Liang, F.K., Yu, X.H., Mu, X.S., Li, S.L., Xu, S.T., Liu, W., Zou, M., 2011. Accommodation zones and their controls on depositional system in the Middle of Third Member of Shahejie Formation, South of Dongpu Sag, Geoscience 25, 1.

Lin, C.S., Yang, H.J., Liu, J.Y., 2009. Paleostructural geomorphology of the Paleozoic central uplift belt and its constraint on the development of depositional facies in the Tarim Basin. Sci. in China 52, 823-834.

Lowe, D.R., 1976. Grain flow and grain flow deposits. J. Sed. Pet. 46, 188-199.

Lowe, D.R., 1982. Sediment gravity flows: II. Depositional models with special reference to the deposits of high-density turbidity currents. J. Sediment. Res.. 52, 279-297.

Mack, G.H., Leeder, M.R., 1999. Climatic and tectonic controls on alluvial-fan and axial-fluvial sedimentation in the Plio-Pleistocene Palomas half graben, southern Rio Grande Rift. J. Sediment. Res. 69, 635-652.

McArthur, A.D., Hartley, A.J., Archer, S.G., Jolley, D.W., Lawrence, H.M., 2016. Spatiotemporal relationships of deep-marine, axial, and transverse depositional systems fromthe synrift Upper Jurassic of the central North Sea. Am. Assoc. Pet. Geol. Bull. 100, 1469–1500.

McKellar, Z., Hartley, A.J., Morton, A.C., Frei, D., 2020. A multidisciplinary approach to sediment provenance analysis of the late Silurian–Devonian Lower Old Red Sandstone succession, northern Midland Valley Basin, Scotland. J. Geol. Soc. London. 177, 297-314.

McLeod, A.E., Underhill, J.R., Davies, S.J., Dawers, N.H., 2002. The influence of fault array evolution on synrift sedimentation patterns: Controls on deposition in the Strathspey-Brent-Statfjord half graben, northern North Sea. Am. Assoc. Pet. Geol. Bull. 86, 1061–1093.

Middleton, G.V., 1970. Experimental studies related to problems of flysch sedimentation. Geol. Assoc. Can. Special Pap. 7, 253-272.

Mulder, T., Migeon, S., Savoye, B., Faugères, J.C., 2001. Inversely graded turbidite sequences in the deep Mediterranean: a record of deposits from flood-generated turbidity currents?. Geo-Mar. Lett. 21, 86-93.

Mulder, T., Syvitski, J.P., Migeon, S., Faugeres, J.C., Savoye, B., 2003. Marine hyperpycnal flows: initiation, behavior and related deposits. A review. Mar. Pet. Geol. 20, 861-882.

Myrow, P.M., Southard, J.B., 1996. Tempestite deposition. J. Sediment. Res. 66, 875-887.

Nadon, G.C., Middleton, G.V., 1985. The stratigraphy and sedimentology of the Fundy Group (Triassic) of the St. Martins area, New Brunswick. Can. J. Earth Sci. 22, 1183-1203.

Olariu, C., Bhattacharya, J.P., 2006. Terminal distributary channels and delta front architecture of river-dominated delta systems. J. Sed. Res. 76, 212–233.

Owen, G., 1995. Soft-sediment deformation in upper Proterozoic Torridonian sandstones (Applecross Formation) at Torridon, northwest Scotland. J. Sediment. Res. 65, 495-504.

Pettijohn, F.J., 1975. Sedimentary Rocks, 3rd ed. Harper and Tow, New York, pp. 628.

Pettijohn, F.J., Potter, P.E., Siever, R., 1987. Sand and sandstone, 2nd ed. Springer-Verlag, pp. 533.

Phillips, E.R. 2007. Petrology and provenance of the Siluro-Devonian (Old Red Sandstone facies) sedimentary rocks of the Midland Valley, Scotland. British Geological Survey Internal Report IR/07/040.

Postma, G., Cartigny, M.J.B., Kleverlaan, K., 2009. Structureless, coarse-tail graded Bouma Ta formed by internal hydraulic jump of the turbidity current? Sediment. Geol. 219, 1-6.

Postma, G., Nemec, W., Kleinspehn, K.L., 1988. Large floating clasts in turbidites; a mechanism for their emplacement. Sediment. Geol. 58, 47-61.

Qi, J., Yang, Q., 2010. Cenozoic structural deformation and dynamic processes of the Bohai Bay basin province, China. Mar. Pet. Geol. 27, 757–771.

Ravnås, R., Steel, R. J., 1997. Contrasting styles of Late Jurassic syn-rift turbidite sedimentation: A comparative study of the Magnus and Oseberg areas, northern North Sea. Mar. Petroleum Geol. 14, 417–449.

Reading, H.G., Collinson, J.D., 1996. Clastic coasts. In: Reading, H.G. (Ed.), Sedimentary Environments: Processes, Facies and Stratigraphy. Blackwell Science, Oxford, pp. 154–231.

Rees, A.I., 1968. The production of preferred orientation in a concentrated dispersion of elongated and flattened grains. J. Geol. 76, 457-465.

Rees, A.I., 1983. Experiments on the production of transverse grain alignment in a sheared dispersion. Sedimentology 30, 437-448.

Renaut, R.W., Gierlowski-Kordesch, E.H., 2010. Lakes. In: James N.P., Dalrymple R.W. (Eds.), Facies Models. Geol. Assoc. Can. IV Series, GEOtext 6, 541–575.

Renaut, R.W., Owen, R.B., 1991. Shore-zone sedimentation and facies in a closed rift lake: the Holocene beach deposits of Lake Bogoria, Kenya. In: Anadon P., Cabrera L., Kelts K. (Eds.), Lacustrine Facies Analysis, Spec. Publ. into Ass. Sediment. 13, 175-195.

Roveri, M., et al., 2014, The Messinian Salinity Crisis: Past and future of a great challenge for marine sciences. Mar. Geol. 352, 25–58.

Sabato, M.M., 2007. Recognition of trigger mechanisms for soft-sediment deformation in the Pleistocene lacustrine deposits of the Sant'Arcangelo Basin (Southern Italy): seismic shock vs. overloading. Sed. Geol. 196, 31–45.

Scholz, C.A., Talbot, M.R., Brown, E.T., Lyons, R.P., 2011. Lithostratigraphy, physical properties and organic matter variability in Lake Malawi Drillcore sediments over past 145,000 years. Palaeogeogr. Palaeoclimatol. Palaeoecol. 303, 38–50.

Schomacker, E.R., Kjemperud, A.V., Nystuen, J.P., Jahren, J.S., 2010. Recognition and significance of sharp-based mouth-bar deposits in the Eocene Green River Formation, Uinta Basin, Utah. Sedimentology 57, 1069–1087.

Schwarz, S., Wood, L., 2016. Drainage Systems in Rift Basins: Implications for Reservoir Quality. AAPG Annual Convention & Exhibition, Calgary, Alberta, Canada.

Sihombing, E.H., Indra, Y., Waworuntu, R.D., Priwastono, D., 2019. The Stratigraphy of a Lacustrine Associated Reservoir in the Belut Formation, Block B, West Natuna Basin. Proceedings, Indonesian Petroleum Association, IPA19-G-437.

Sirota, I., Enzel, Y., Lensky, N.G., 2018, Halite focusing and amplification of salt thickness: From the Dead Sea to deep hypersaline basins. Geology 46, 851–854.

Slatt, R.M., Eyles, N. 1981. Petrology of glacial sands: implications for the origin and mechanical durability of lithic fragments. Sedimentology 28, 171–183.

Smith, D.G., Jol, H.M., Smith, N.D., Kostaschuk, R.A., Pearce, C.M., 2005. The wave-dominated Willial River Delta, Lake Athabasca, Canada: its morphology, radar stratigraphy, and history. In: Giosan L., Bhattacharya J.P. (Eds.), River Deltas-Concepts, Models, and Examples. SEPM Spec. Publ. 83, 101–123.

Somerville, D.J.P., Mountney, N.P., Colombera, L., Collier, R.E.L., 2020. Impact of a pre-existing transverse drainage system on active rift stratigraphy: An example from the Corinth Rift, Greece. Basin Res. 32, 764–788.

Song, H.Y., 2016. Reservoir characterization of the 3rd Member of the Shahejie Formation, Dongpu Depocentre, Bohai Bay Basin, China. Unpublished Master Thesis, China University of Petroleum (Beijing).

Soreghan, M.J., Scholz, C.A., Wells, J.T., 1999. Coarse-grained, deep-water sedimentation along a border fault margin of Lake Malawi, Africa; seismic stratigraphic analysis. J. Sediment. Res. 69, 832-846.

Su, H., Qu, L.P., Zhang, J.C., Wang, P.X., He, F., Wang, M., Wang, Q., Hu, Y.J., 2006. Tectonic evolution and extensional pattern of rifted basin, a case study of Dongpu depression. Oil Gas Geol. 27, 70-71 (in Chinese with English abstract).

Surlyk, F., 1978. Submarine fan sedimentation along fault scarps on tilted fault blocks (Jurassic-Cretaceous boundary, East Greenland). Grønl. Geol. Unders. Bull. 128, 1-108.

Surlyk, F., 1984. Fan-delta to submarine fan conglomerates of the Volgian-Valanginian Wollaston Forland group, east Greenland. In: Koster, E.H., Steel, R.J. (Eds.), Sedimentology of Gravels and Conglomerates, pp. 359-382. Mere. Can. Soc. Pet. Geol. 10.

Swift, D.J.P., Thorne, J.A., 1991. Sedimentation on continental margins, I: a general model for shelf sedimentation. In: Swift, D.J.P., Oertel, G.F., Tillman, R.W., Thorne, J.A. (Eds.), Shelf Sand and Sandstone Bodies: Geometry, Facies and Sequence Stratigraphy. IAS Spec. Publ. 14, 3-31.

Syvitski, J.P.M., Milliman, J.D., 2007. Geology, geography, and humans battle for dominance over the delivery of fluvial sediment to the coastal ocean. J. Geol. 115, 1–19.

Tänavsuu-Milkeviciene, K., Sarg, J.F., 2012, Evolution of an organic-rich lake basin: Stratigraphy, climate and tectonics: Piceance Creek basin, Eocene Green River Formation. Sedimentology 59, 1735–1768.

Tang, L., Pang, X., Xu, T., Hu, T., Pan, Z., Guo, K., Yu, R., Shao, X., Zhang, X., Xu, Y., 2017. Hydrocarbon generation thresholds of Paleogene Shahejie Fm source rocks and their north–south differences in the Dongpu Sag, Bohai Bay Basin. Nat. Gas. Ind. 37, 26–37.

Tang, L., Song, Y., Pang, X., Jiang, Z., Guo, Y., Zhang, H., Pan, Z., Jiang, H., 2020. Effects of paleo sedimentary environment in saline lacustrine basin on organic matter accumulation and preservation: A case study from the Dongpu Depression, Bohai Bay Basin, China. J. Pet. Sci. Eng. 185, 106669.

Turner, C., Allen, P. A., 1991. The Central Brae Field, block 16/7a, UK North Sea. In: Abbotts, I. (Ed.), United Kingdom Oil and Gas Fields; 25 years Commemorative Volume. Geol. Soc. Lond. Mem. 14, 49–54.

Turner, C.C., Bastidas, R.E., Connell, E.R., Petrik, F.E., 2018. Proximal submarine fan reservoir architecture and development in the Upper Jurassic Brae Formation of the Brae fields, South Viking Graben, UK North Sea. In: Turner, C.C., Cronin B.T. (Eds.), Rift related coarse-grained submarine fan reservoirs; The Brae Play, South Viking Graben, North Sea. AAPG Mem., Tulsa, OK, AAPG, 115, 213–256.

Vail, P.R., Mitchum, R.M., Thompson, S. III, 1977. Seismic stratigraphy and global changes of sea-level, part 4: global cycles of relative changes of sea-level. In: C. E. Payton (Ed.) Seismic Stratigraphy-Applications to Hydrocarbon Exploration. Am. Assoc. Petrol. Geol. Mem. 26, 83–-97.

Walker, R.G., Duke, W.L., Leckie, D.A., 1983. Hummocky stratification: Significance of its variable bedding sequences: Discussion and reply: Discussion. Geol. Soc. Am. Bull. 94, 1245-1249.

Wang, M., Chen, H., Huang, C., Kemp, D.B., Xu, T., Zhang, H., Li, M., 2020. Astronomical forcing and sedimentary noise modeling of lake-level changes in the Paleogene Dongpu Depression of North China. Earth Planet. Sci. Lett. 535, 116116.

Wellner, R., Beaubouef, R., Van Wagoner, J., Roberts, H., Sun, T., 2006 Jet-plume depositional bodies – the primary building blocks of Wax Lake Delta. Gulf Coast Assoc. Geol. Soc. Trans. 55, 867–909.

Wyllie, M.R.J., Gregory, A.R., Gardner, L.W., 1956. Elastic wave velocities in heterogeneous and porous media. Geophysics 21, 41-70.

Ye, J.R., Sun, J.Z., Yang, X.H., 2008. The control of faults on sedimentation and hydrocarbon accumulation in the western slope zone of Dongpu Sag. Unpublished internal report, Research Institute of Exploration and Development, Zhongyuan Oilfield, Sinopec, China.

Young, M.J., Gawthorpe, R.L., Sharp, I.R., 2000. Sedimentology and sequence stratigraphy of a transfer zone coarse-grained delta, Miocene Suez Rift, Egypt. Sedimentology 47, 1081–1104.

Yu, H.B., Cheng, X.S., Qi, J.F., 2019. Control of fault activity on sedimentation of Paleogene in Dongpu Sag. Lithologic Reservoirs 31, 12-23.

Yu, X.H., Li, S.L., Liang, F.K., Zou, M., Chen, B.T., Li, H.M., Liu, W., Wang, N., 2012. Palaeogeographic reconstruction of the 3rd Member of the Shahejie Formation, Dongpu Depocentre, Bohai Bay Basin, China. Unpublished internal report, China University of Geosciences (Beijing).

Zhang, X., Scholz, C.A., 2015. Turbidite systems of lacustrine rift basins: Examples from the Lake Kivu and Lake Albert rifts, East Africa. Sediment. Geol. 325, 177–191.

Zhu, Y., Liu, S., Zhang, B., Gurnis, M., Ma, P., 2020. Reconstruction of the Cenozoic deformation of the Bohai Bay Basin, North China. Basin Res. 1–18.